

Lidar survey of the Joggins Formation in the Coal Mine Point section, Cumberland Basin (Nova Scotia, Canada)

CARLOS WONG

SUPERVISOR DR. GRANT WACH

Submitted in Partial Fulfilment of the Requirements

for the Degree of Bachelors of Science

Department of Earth Science

Dalhousie University, Halifax, Nova Scotia

April, 2014

DATE: April 16, 2014

AUTHOR: Juan Carlos Wong

TITLE: Lidar survey of the Joggins Formation in
the Coal Mine Point section, Cumberland
Basin (Nova Scotia, Canada)

Degree: B.Sc Convocation: May Year: 2014

Permission is herewith granted to Dalhousie University to circulate and to have copied for non-commercial purposes, at its discretion, the above title upon the request of individuals or institutions.



Signature of Author

THE AUTHOR RESERVES OTHER PUBLICATION RIGHTS, AND NEITHER THE THESIS NOR EXTENSIVE EXTRACTS FROM IT MAY BE PRINTED OR OTHERWISE REPRODUCED WITHOUT THE AUTHOR'S WRITTEN PERMISSION.

THE AUTHOR ATTESTS THAT PERMISSION HAS BEEN OBTAINED FOR THE USE OF ANY COPYRIGHTED MATERIAL APPEARING IN THIS THESIS (OTHER THAN BRIEF EXCERPTS REQUIRING ONLY PROPER ACKNOWLEDGEMENT IN SCHOLARLY WRITING) AND THAT ALL SUCH USE IS CLEARLY ACKNOWLEDGED.

DALHOUSIE UNIVERSITY
DEPARTMENT OF EARTH SCIENCES

The readers of this thesis entitled “Lidar survey of the Joggins Formation in the Coal Mine Point section, Cumberland Basin (Nova Scotia, Canada)” by Juan Carlos Wong in partial fulfillment of the requirements for the degree of Bachelors of Science are the following.

Supervisor: Dr. Grant Wach

Coordinator: Dr. Martin Gibling

Reader: Dr. John Gosse

Abstract

The Carboniferous Joggins Formation outcrops along the shoreline of Chignecto Bay (Nova Scotia, Canada). The area of the Joggins Fossil Cliffs (UNESCO World Heritage Site) presents an outstanding set of channel and floodplain deposits, and fossilized tree trunks. This study focuses on the Coal Mine Point reference section, which comprises interbedded sandstone, shale and coal seams, and where accommodation was created by halokinetic activity (salt withdrawal). This study uses lidar to interpret the outcrop, augmented with gamma-ray and permeability data. Currently Joggins Fossil Cliffs records fossilized trees with a measured section log. With the use of lidar and spatially-calibrated Differential Global Positioning System (DGPS) to capture high-resolution images of meanderbelt channel architecture and fossils of upright lycopsids and calamitaleans. This imaging technique is an innovative approach and utilizes new technologies to provide a high-resolution 3D survey of the cliff (4 mm resolution at 100 m) detailing of channels and fossil tree trunks. Using the 3D survey coupled with other tools including scintillometer and permeameter, we can supplement data from the lidar scan and increase confidence of interpretations. Scintillometer measurements recorded at outcrop are used to generate a pseudo-gamma log and permeameter measurements were recorded to understand permeability of the corresponding lithologies. Lidar provided important information for rock properties and high detail of the outcrop that can be used in the assessment of the reservoir characteristics of the Joggins Formation in Cole Mine Point section. Annual lidar surveys with scintillometer and permeameter will provide an informative data set to continue analysis and interpretations of the Joggins Fossil Cliffs.

Keywords: Bay of Fundy, Cumberland Basin, Joggins Fossil Cliffs, Joggins Formation, Carboniferous, Reservoir Characterization, Digital Outcrop Models, Permeability, Gamma-Ray, Lidar

Table of Contents

Abstract.....	iv
Table of Contents.....	v
Table of Figures.....	vii
Table of Tables.....	x
List of Abbreviations.....	xi
Acknowledgements.....	xii
1 Introduction.....	1
1.1 Purpose.....	1
1.2 Geographical and Geomorphological Setting of the Study Area.....	2
1.3 Geological Background.....	5
1.3.1 Cumberland Basin.....	5
1.3.2 Joggins Formation.....	7
1.3.3 Preservation of the Flora.....	9
1.3.4 Meanderbelt Channels.....	13
2 Methods and Data Processing.....	15
2.1 Differential Global Positioning System (DGPS).....	15
2.2 Light Detection and Ranging (lidar).....	17
2.3 Scintillometer.....	21
2.4 Permeameter.....	22
2.5 Data Processing.....	23
2.5.1 ArcGIS.....	23
2.5.2 Petrel.....	24
3 Results.....	25
3.1 Differential Global Positioning System (DGPS).....	25
3.2 Light Detection and Ranging (lidar).....	27

3.3	Scintillometer	28
3.4	Permeameter	31
3.4.1	Hand Samples.....	32
3.5	Petrel.....	39
4	Discussion.....	43
4.1	Light Detection and Ranging (lidar)	43
4.1.1	Digital Outcrop Model (DOM).....	43
4.1.2	Fossil Tree Identification in DOM.....	43
4.1.3	Lithological Identification.....	44
4.2	Gamma-ray and permeability	46
4.3	Integrated Reservoir Characterization.....	47
5	Conclusion and Recommendation	48
5.1	Conclusion.....	48
5.2	Recommendations and Future Work.....	49
5.2.1	3D Visualization.....	50
6	References	52
7	Appendix	55
7.1	Complete measured stratigraphic section of the Joggins Formation at Coal Mine Point	56

Table of Figures

Figure 1.1 - Location of Dalhousie University (Green Pin), the Joggins Fossil Cliff Center (Red Pin).....	2
Figure 1.2 – Joggins Formation and Quaternary sediments (red). Both units are separated by an angular unconformity (yellow dashed line). Coal Mine Point, Joggins, Cumberland Basin, Nova Scotia, Canada....	3
Figure 1.3 – Aerial view of the area surrounding Joggins Fossil Cliffs Center. Due to the contrasting lithologies there are areas of low vs. high erosion rate. lidar location during data acquisition is marked with X.	3
Figure 1.4 - Jointing and fractures with fallen blocks within the Joggins Formation at Coal Mine Point (Cumberland Basin, Nova Scotia).....	4
Figure 1.5 - Fallen blocks at the toe of the promontory of Coal Mine Point (Cumberland Basin, Nova Scotia).	5
Figure 1.6 - Schematic representation of a salt withdrawal system; salt moves out as more pressure from accumulated sediments is applied to the overlying the salt system.....	6
Figure 1.7 – General paleogeography of the Cumberland Basin during the Pennsylvanian, Carboniferous. Joggins Fossil Cliffs Center location within the Carboniferous Pennsylvanian Lowlands within the Cumberland Basin formed.....	6
Figure 1.8 – Carboniferous stratigraphy of the Cumberland Basin and simplified geological map of the area of Joggins Fossil Cliffs Center.	7
Figure 1.9 – Limestone and coal thickness with facies associations correlated to relative base level for the Joggins Formation. Note the thick sandstone preserved at Coal Mine Point separate cycles 9 and 10, and was deposited when the region was a poorly drained floodplain. Approximate range of interest for this study denoted with red box. (OWFA: Open Water Floodplain Area. PDFFA: Poorly Drained Floodplain Area. WDFA: Well Drained Floodplain Area).....	8
Figure 1.10 – Sedimentary and stratigraphical characteristics of the Joggins Formation at Cole Mine Point. Blue line: Quaternary Unconformity, yellow arrows: channel bodies, red arrow: interbedded shale, green circles: preserved tree.....	9
Figure 1.11- Fossil tree within the Joggins Formation at Coal Mine Point (Cumberland Basin, Nova Scotia).	10
Figure 1.12 – Schematic representation of channel architecture and faunal dynamics during the deposition of the Joggins Formation during the Carboniferous (Cumberland Basin, Nova Scotia).	10
Figure 1.13 - (A) Cast of a <i>Calamites</i> and (B) Mold and cast of a <i>Sigillaria</i>	11

Figure 1.14 - <i>Alethopteris</i> coal imprint (dark leaf like shapes) on rock surface, sample from Dalhousie University, Earth Science Department.....	11
Figure 1.15 - <i>Calamites</i> Fossil, sample from Dalhousie University, Earth Science Department.....	12
Figure 1.16 - Highlight of diamond shape pattern within the bark of <i>Lepidodendron</i> , sample from Dalhousie University, Earth Science Department.....	12
Figure 1.17 - Highlight of honeycomb shape pattern within the bark of <i>Sigillaria</i> , sample from Dalhousie University, Earth Science Department.....	13
Figure 1.18 - The architecture and flow regime of a meander channel (modified from Prothero & Schwab, 2004)	14
Figure 2.1 – DGPS base station.	15
Figure 2.2 – DGPS rover.	16
Figure 2.3 - Multipath effect of GPS, creating errors within the GPS device.....	16
Figure 2.4 – Targets used for georeferencing. The targets have high reflective background (reflective black) contrasted with a less reflective centre circle, design by Johnathan Thibodeau.	17
Figure 2.5 - Optech in. ILRIS HD lidar on a tripod, performing a scan.	18
Figure 2.6 - The intensity property corresponds to the intensity of the reflected laser pulse which depends on the lithology of the surface reflecting the beam. A laser pulse is emitted from the source towards the outcrop. As the pulse reflects from the outcrop it returns back to the source. During the reflection some intensity of the pulse is lost.	19
Figure 2.7 – Photomontage depicting the Coal Mine Point study area taken from the intertidal zone by the lidar. The lidar scanned a total of four segments for this section and for each segment a digital photograph is recorded. The four photographs are compiled here.....	19
Figure 2.8 - Angle of dispersion of laser beam. As the laser pulse source is at a further distance from the outcrop, the horizontal distance between each laser pulse increases, in turn reducing the image resolution.....	20
Figure 2.9 – An example of a shadow zone. An overhang is obstructing the path of the laser pulse. Resulting in an area with no data. The red line is the intended area of capture along the outcrop. The grey area is the portion of the outcrop where no data are collected.....	21
Figure 2.10 - Handheld Scintillometer, it measures the spectral gamma emission of the formation (K, U, Th)	21
Figure 2.11 – Schematic representation of permeability.	22

Figure 2.12 – Pneumatic device to measure permeability of the rock, in mD this is a TinyPerm II by New England Research Inc. 23

Figure 2.13 - TinyPerm II Permeability Calibration Graph. T: TinyPerm II reading K: Permeability Value (mD). 23

Figure 2.14 - NASA JPL library spectroscopy, solid sample data showing median (solid line) and quartiles (dashed lines) for shale (gray) and sandstone (black). The dashed line is the approximate wavelength of terrestrial lidar. Note the spectral separability between sandstones and shale at different wavelengths. 24

Figure 3.1 - File format of an XYZ output from Optech Inc. parser, based on data collected for this study. 27

Figure 3.2 – Unprocessed lidar scan after import into ArcScene. Each colour represents a different scan section; 4 sections total. Red pins indicate the location of the georeference targets in the scan..... 28

Figure 3.3 - Scintillomer measurements of the Joggins Formation at Coal Mine Point section. Figures A and B. 29

Figure 3.4 – Correlation of pseudo gamma-ray with the measured stratigraphic section of the Joggins Formation at Coal Mine Point. Gamma Ray is representative of the lithology. 30

Figure 3.5 - Petrel render of the data set. The warmer yellow and red hues indicates higher intensity values due to the greater reflectivity of the quartz component in the sandstones Red arrow indicates north and the horizontal distance. 40

Figure 3.6 – Petrel render image of the data set. Quaternary Unconformity (green dash line), mine tailings (red arrow) and vegetation (blue arrow)..... 41

Figure 3.7 - Petrel render image of the data set. Where is possible to identify shales (baffle and barriers, red arrow) and sandstones (reservoirs, green arrow). Reflective intensity differences indicates shales. These shales form barriers or baffles to fluid flow between the sandbodies which are the high reflective images. 41

Figure 3.8 - (A) Fossil trees within succession of sediments in a digital photograph. (B) The same fossil trees within the DOM of these same successions. For closer view of preserved tree see Figure 1.11. 42

Figure 4.1 - Petrel render image of the data set, showing a concave geometry (red arrow) in outcrop. The concave shape acts as an amplifier of the laser pulse, resulting in higher intensities within the concave shape. This is noted by the warmer red colours..... 45

Figure 4.2 - Petrel render image of the data set, showing small promontories (inside white box) in outcrop. The promontories deflect the laser pulse, resulting in lower intensities within the promontory shape. This is noted by the grey colours..... 45

Figure 4.3 - (A) Petrel render of the data set depicting connected sandbodies (Warm red and yellow colours). (B) Digital Photograph of outcrop showing non-connected sandbodies. Dashed line represents the false intensity error that the lidar has recorded. 46

Figure 4.4 - Petrel render image of the data set, measuring 3 different reservoirs separated by thick shales. The reservoirs units are noted to be 8 m, 23 m and 8 m. Within each reservoir shale baffles and barriers are noted to separate connectivity between sandstone channels. 47

Figure 5.1 – To build a 3D model of the study area multiple scans must be completed and compiled to both generate a true representation of the Joggins Formation and to measure coastal erosion rates. ... 50

Figure 5.2 – A car service manual using augmented reality. 51

Table of Tables

Table 3.1 – Location of the lidar setup near Coal Mine Point. 25

Table 3.2 - Location of the left georeferencing Target 1 as viewing the cliff face from the water. 26

Table 3.3 - Location of the georeferencing Target 2 as viewing the cliff face from the water..... 26

Table 3.4 - Location of the georeferencing Target 3 as viewing the cliff face from the water..... 27

Table 3.5 – Scintillometer measurements collected at Coal Mine Point with corresponding lithological descriptions..... 29

Table 3.6 - Permeability measurements of Coal Mine Point and its ranking according to Table 3.7..... 31

Table 3.7 - Ranking of Permeability (K) (Nebaway, Rochette, & Geraud, 2009). 31

List of Abbreviations

3D	3-DIMENSION
API	AMERICAN PETROLEUM INSTITUTE STANDARDIZED UNIT
ASCII	AMERICAN STANDARD CODE FOR INFORMATION INTERCHANGE
cps	COUNTS PER SECOND
CSV	COLUMN SPACED VALUES
DGPS	DIFFERENTIAL GLOBAL POSITION SYSTEM
DOM	DIGITAL OUTCROP MODEL
GIS	GEOGRAPHIC INFORMATION SYSTEM
GPS	GLOBAL POSITION SYSTEM
JFCC	JOGGINS FOSSIL CLIFF CENTRE
LCD	LIQUID CRYSTAL DISPLAY
Lidar	LIGHT DETECTION AND RANGING
mD	MILIDARCY UNIT
PCD	POINT CLOUD DATA
UNESCO	UNITED NATIONS EDUCATIONAL, SCIENTIFIC AND CULTURAL ORGANIZATION

Acknowledgements

I want to thank my research supervisor, Dr. Grant Wach, for the opportunity to be part of the Basin and Research Lab, and for the amazing project this thesis is about. Dr. Wach, whose encouragement and guidance I will never forget, has guided me through hurdles and all the obstacles in the completion of this research project.

I want to thank Jenna Boon, Melissa Grey and the staff at Joggins Fossil Cliff Center for welcoming us to do research in this wonderful UNESCO site.

I want to thank Dr. Ricardo Silva, Darragh O'Connor, Carla Dickson, and Trevor Kelly for their continuous support and ideas to the research project. They have shared valuable insights in the relevance of the study.

I want to thank the entire staff at the Basin and Research Lab for making me feel at home and supported when I needed the most.

I want to thank my colleagues in Earth Science and in Computer Science for encouraging me to complete this study.

Last but not least, to my sisters and mother for supporting me throughout this last year of my undergrad degree.

1 Introduction

1.1 Purpose

Light Detection and Range (lidar) is an innovative technique which has been used in academic and industry geologic studies for the digital capture of outcrop characteristics with unprecedented resolution and accuracy. Previous studies using lidar in Earth Sciences provided higher resolution analysis of rock properties, geomorphology, and coastal erosion allowing enhanced interpretation of processes and properties (Burton, et al. 2011; Buckley, et al. 2013). In Nova Scotia, Rafuse (2011) and Kelly (2014) used lidar for digital rendering and interpretation of the reservoir characteristics of the meander belt successions of the Carboniferous Joggins Formation of the Cumberland Basin (Chignecto Bay, Nova Scotia, Canada).

The objective of this work, developed on the outcrops of the Joggins Formation of the Coal Mine Point section (Joggins Fossil Cliffs, UNESCO World Heritage Site), is to investigate how lidar can be used to define the high-resolution stratigraphy of the fluvial systems by answering the following questions:

- a) Is lidar capable of aiding in the identification of different lithofacies at Joggins?
- b) Can lidar identify fossilized trees within the Joggins Formation?
- c) Can lidar help characterize reservoir connectivity in meander belt systems?
- d) Can lidar data integrated with outcrop observation, gamma-ray and permeability data aid in the interpretation of stratigraphical and sedimentological features of hydrocarbon reservoirs?

This work is also part of an ongoing study aimed to characterize Carboniferous tree density within the Joggins Formation and measure the rates of erosion of seaside cliffs near the town of Joggins through the capture of annual lidar scans of the Joggins Formation outcrops.

1.2 Geographical and Geomorphological Setting of the Study Area

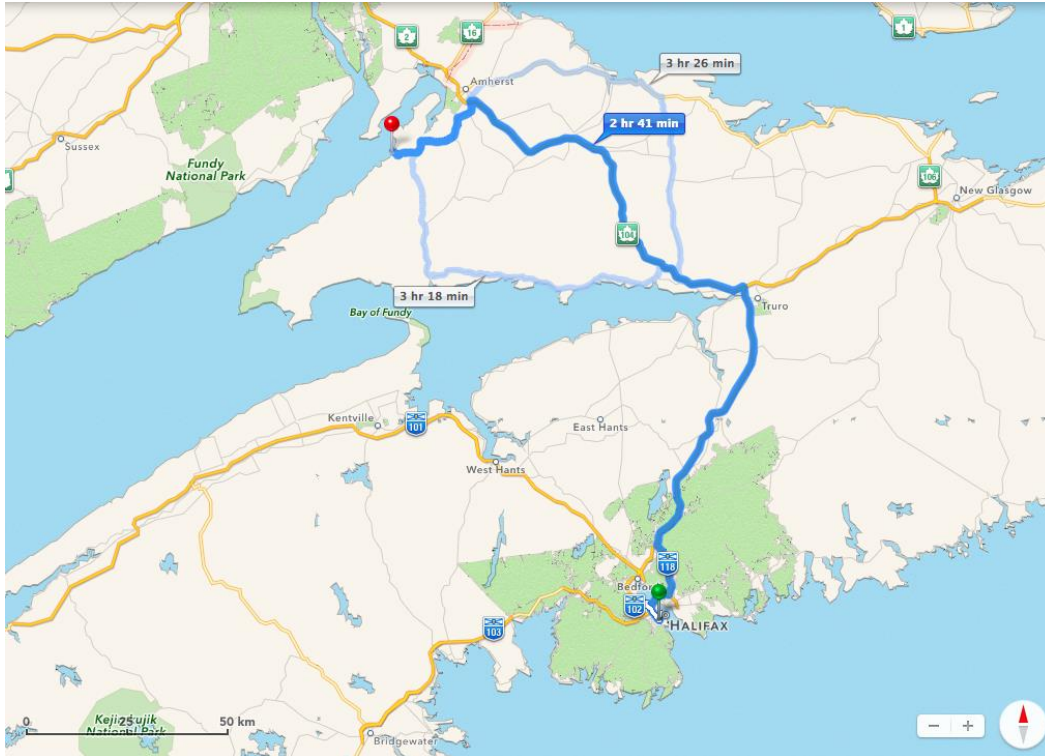


Figure 1.1 - Location of Dalhousie University (Green Pin), the Joggins Fossil Cliff Center (Red Pin) (Apple Inc., 2014).

Located between the provinces of New Brunswick and Nova Scotia, Chignecto Bay is an inlet of the Bay of Fundy (Figure 1.1). It is also part of the Gulf of Maine Watershed. Chignecto Bay is world-renowned due to the Joggins Fossil Cliffs, Canada and the country's 15th UNESCO World Heritage Site.

The Coal Mine Point section is located along the south coastal margin of the Chignecto Bay (Nova Scotia) (UTM coordinates: Zone 20T, Easting 387128 m, and Northing 5061142). Known locally as Hardscrabble Point, this section is approximately 250 m long (Figure 1.1 & Figure 1.2) and is continually exposed to harsh weather conditions. The high (energy) tides coupled with the different resistance to weathering of the different lithologies creates several zones of low vs. high cliff retreat rate (Figure 1.3). Other contributing factors to coastal erosion include wave action but in the Joggins area the high tidal range and storm activity are the dominant factors acting upon the sands and shale intervals on the cliff face. This results in a complex costal pattern (promontory), conditioning assess of people and equipment.



Figure 1.2 – Joggins Formation and Quaternary sediments (red). Both units are separated by an angular unconformity (yellow dashed line). Coal Mine Point, Joggins, Cumberland Basin, Nova Scotia, Canada.

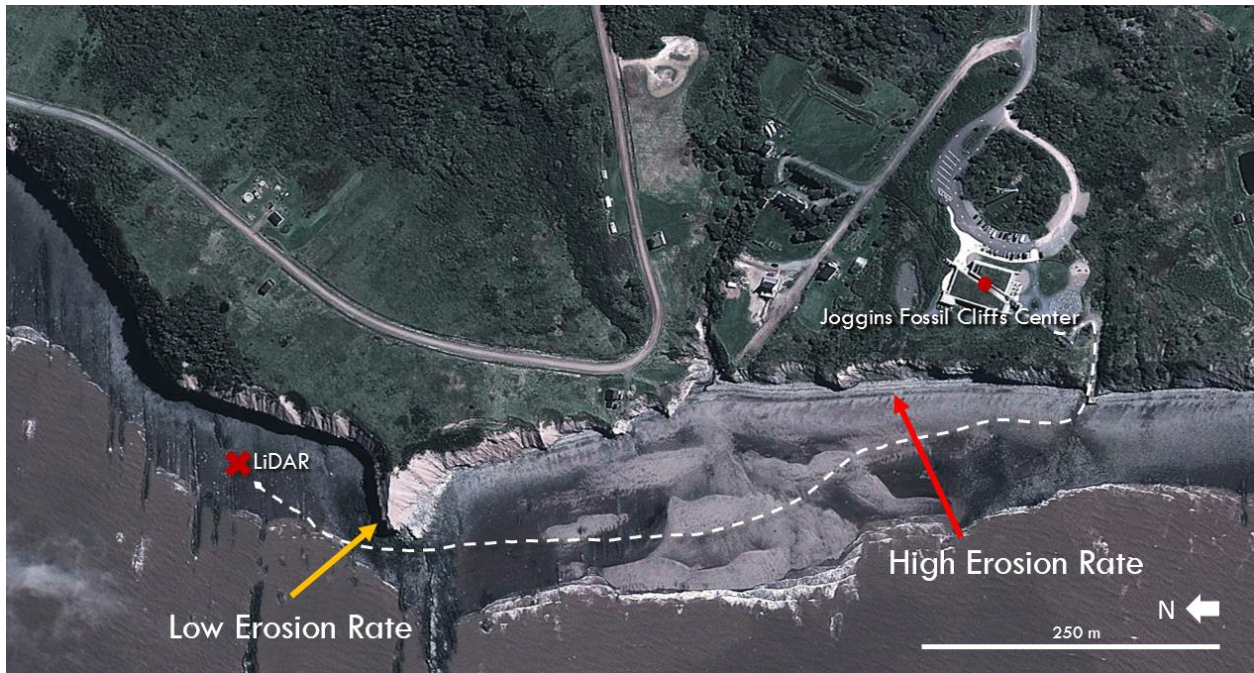


Figure 1.3 – Aerial view of the area surrounding Joggins Fossil Cliffs Center. Due to the contrasting lithologies there are areas of low vs. high erosion rate. Lidar location during data acquisition is marked with X (Google Inc., 2014).

The entire outcrop is very unstable due to jointing and fractures, contributing to the erosion observed along the shoreline. Joint trends are predominantly perpendicular to bedding (decametric to metric spacing). In some locations, larger, outcrop scale, fractures are observed, with large boulders of fallen blocks from the cliff (Figure 1.4 & Figure 1.5). These fractures are expanded by the constant freezing and thawing cycles, and rainfall resulting in collapse of sections of the cliff. The promontory known as Coal

Mine Point results from the lithological contrast from a thick sandstone body, known locally as “reef” and the more argillaceous framing lithofacies (Figure 1.3).



Figure 1.4 - Jointing and fractures with fallen blocks within the Joggins Formation at Coal Mine Point (Cumberland Basin, Nova Scotia).



Figure 1.5 - Fallen blocks at the toe of the promontory of Coal Mine Point (Cumberland Basin, Nova Scotia).

1.3 Geological Background

1.3.1 Cumberland Basin

The Cumberland Basin was formed by cyclic and rapid subsidence controlled by salt withdrawal (halokinesis) (Davies, et al., 2005) and is an excellent example of a salt withdrawal system. Halokinesis is when massive and rapid deposition of sediments occurs on top of evaporites causing the movement of the salt (Waldron & Rygel, 2005) (Figure 1.6). This movement is usually ductile-brittle, within shallow crust, about 8-15 km deep (Jackson, et al., 1994).

Halokinesis created accommodation in the basin that allowed for more sediment to be deposited, sourced from the highlands of the Appalachian Orogen and Gondwanan upland (Figure 1.7). This extensional tectonic event created an uneven topography of fault blocks in the region by the deformation of the overburden. The Joggins Formation shows the displacement of salt movement to be at least 1 km. Subsidence was episodic, with optimal conditions for peat accumulation and entombment of the flora (Waldron & Rygel, 2005). The rate of sedimentation in the Cumberland Basin is believed to be higher than

average compared with other coal-bearing Carboniferous units (McCabe, 1991), and the deposition of the Joggins Formation was close to the water surface (Davies & Gibling, 2003).

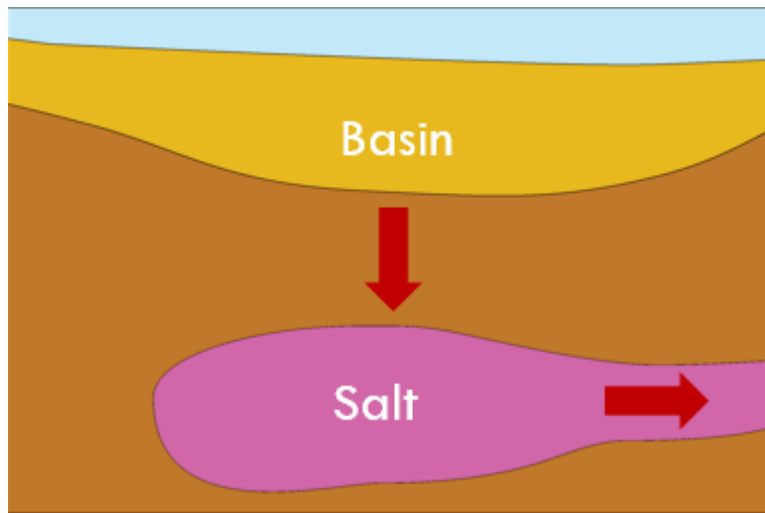


Figure 1.6 - Schematic representation of a salt withdrawal system; salt moves out as more pressure from accumulated sediments is applied to the overlying the salt system.

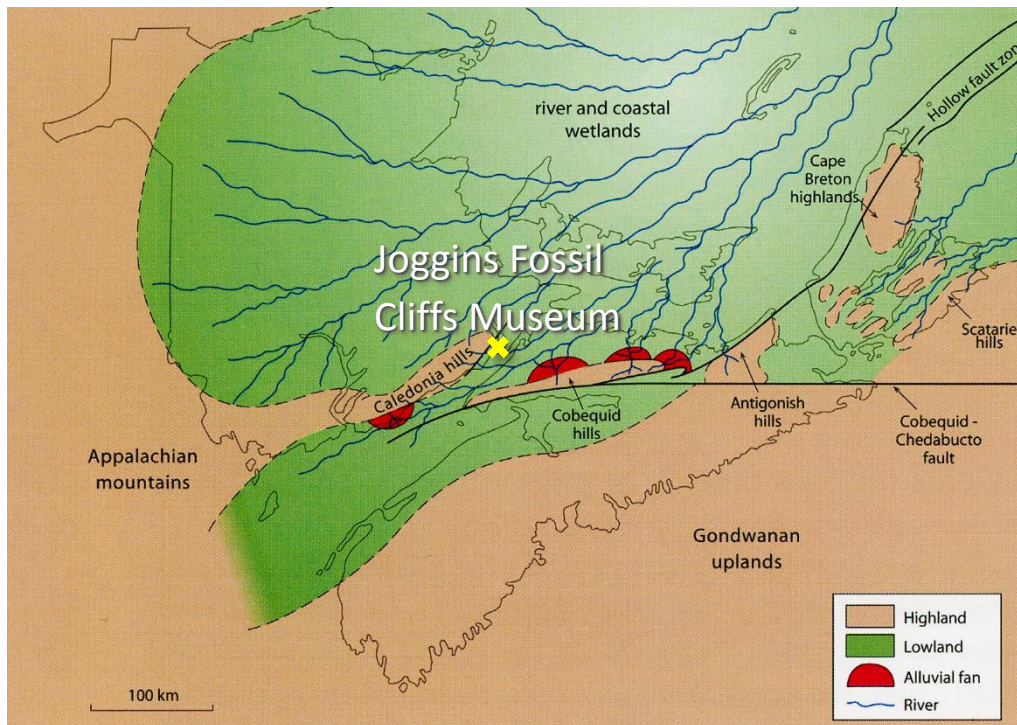


Figure 1.7 – General paleogeography of the Cumberland Basin during the Pennsylvanian, Carboniferous. Joggins Fossil Cliffs Center location within the Carboniferous Pennsylvanian Lowlands within the Cumberland Basin formed (modified from Fensome & Williams, 2001).

1.3.2 Joggins Formation

The Joggins Formation rests between the Spring Hill Mines and the Little River formations, all part of the Cumberland Group (Figure 1.8). The Little River Formation underlies the Joggins Formation and is measured as 635.8 m thick. The Springhill Mines Formations overlies the Joggins Formation and comprises red beds and thick coals, and is about 714 m thick (Rygel, 2010).

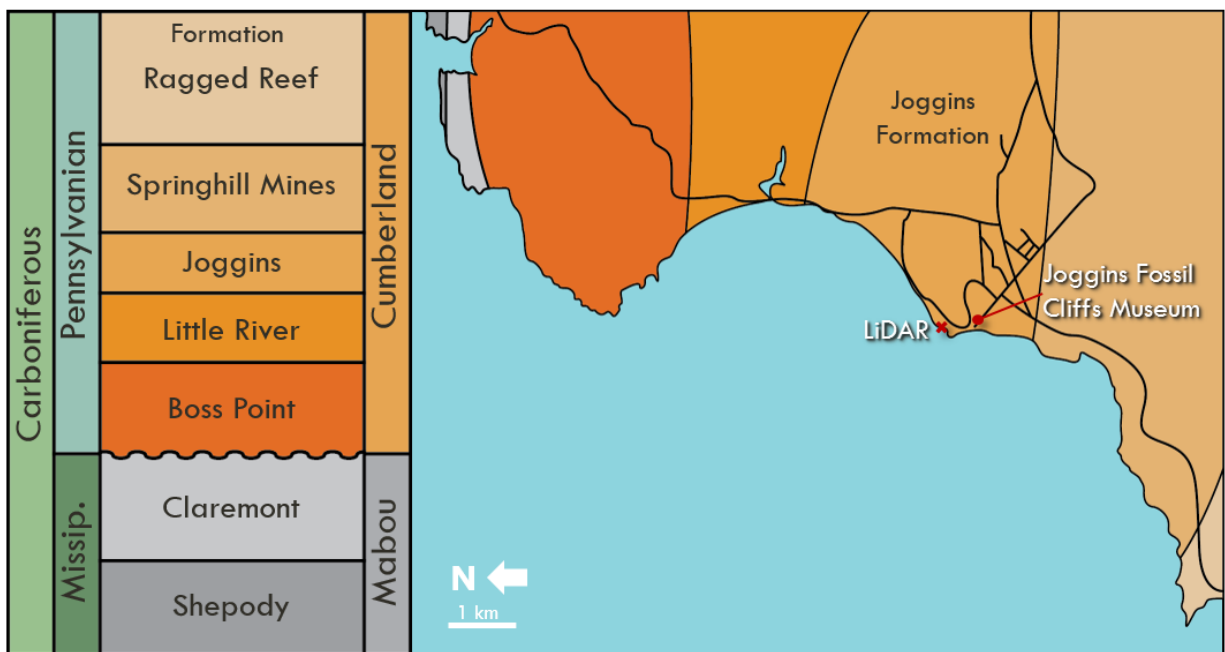


Figure 1.8 – Carboniferous stratigraphy of the Cumberland Basin and simplified geological map of the area of Joggins Fossil Cliffs Center (modified from Grey & Finkel, 2011).

The Joggins Formation comprises shales, coal seams and red beds, dipping 20° S (Figure 1.2). It is about 915.5 m thick and it comprises a multi cycle open-water facies with large distributary meander belt channel systems that is overlain by a thick coal bearing section (Davies, et al., 2005). There are intervals of fossilized tree trunks. A total of 14 cycles were recognized within this unit in previous studies (Davies, et al., 2005) (Figure 1.9), ranging from 16 to 212 m thick with an average of 65 m. A cycle begins with well-developed open-water facies with limestones, mud drapes, trace fossils, and large distributary channel bodies (Davies, et al., 2005). Coal Mine Point corresponds to the base of cycle 10 (Figure 1.9). The coal seams in this formation reach up to 1.7 m, marking a period of wetland conditions (Calder, 2006). The absence of pronounced sequence boundaries and deep-water deposits, as well as the rheotrophic (swamp or boggy ground that is feed by fresh water flow) nature of the precursor peats, suggests that the sediment surface remained close to relative base level through the deposition of the Joggins Formation (Davies & Gibling, 2003). This suggests that accommodation space kept pace with sediment supply, creating an

overall aggradational succession. The sedimentation rates according to Rygel (2005) is between 50 mm/yr - 120 mm/yr.

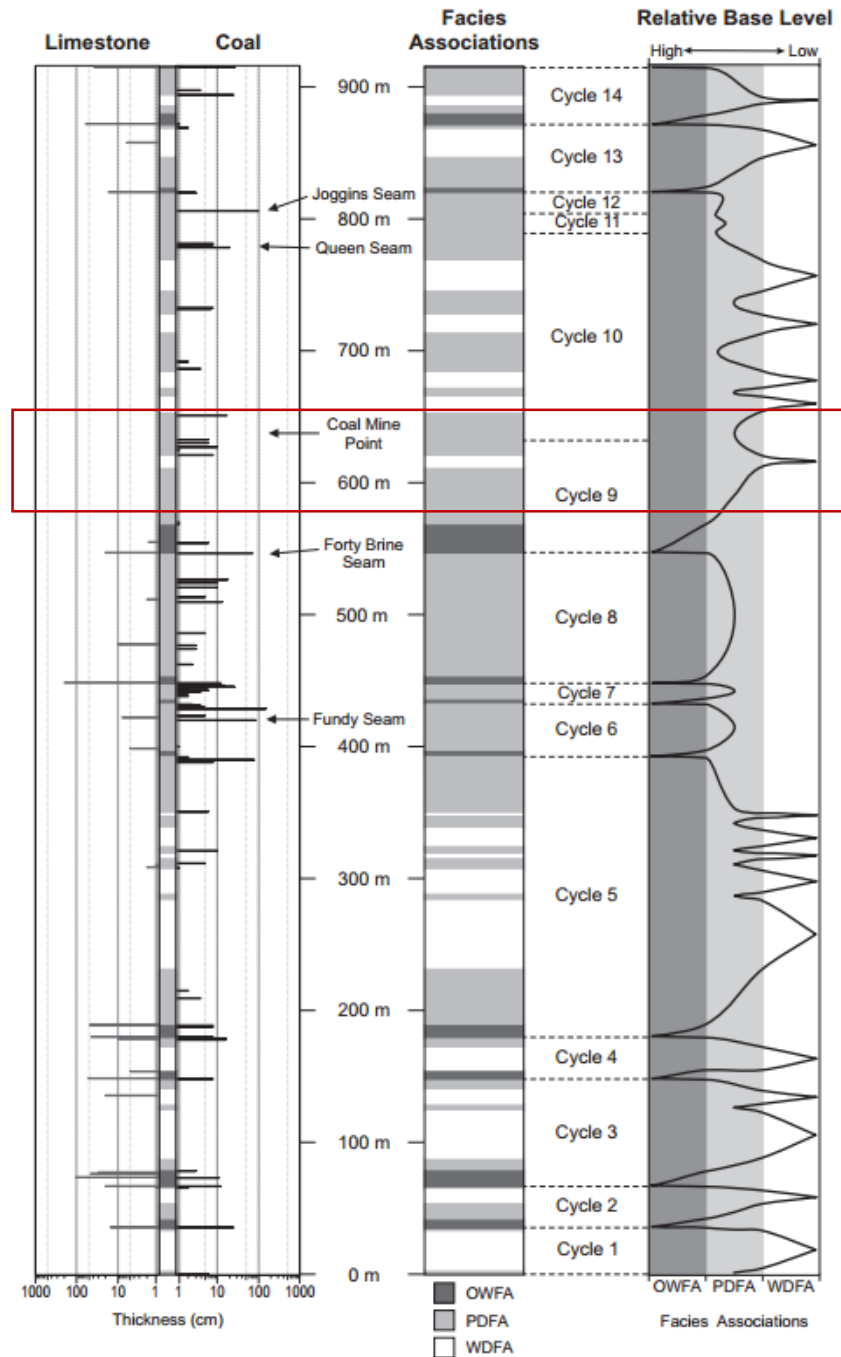


Figure 1.9 – Limestone and coal thickness with facies associations correlated to relative base level for the Joggins Formation. Note the thick sandstone preserved at Coal Mine Point separate cycles 9 and 10, and was deposited when the region was a poorly drained floodplain. Approximate range of interest for this study denoted with red box. (OWFA: Open Water Floodplain Area. PDFA: Poorly Drained Floodplain Area. W DFA: Well Drained Floodplain Area) (modified from Davies et al, 2005).

1.3.3 Preservation of the Flora

As the Cumberland Basin developed, there were periods of rapid sedimentation, burial and preservation, entombing the flora in upright position (Figure 1.10 & Figure 1.11). This process was cyclical, sediments accumulated and new flora established itself (Figure 1.12). Burial and reservation of lycopsid trees in upright position suggest that burial was due to episodic floods with high sediment load (Calder, 2006).

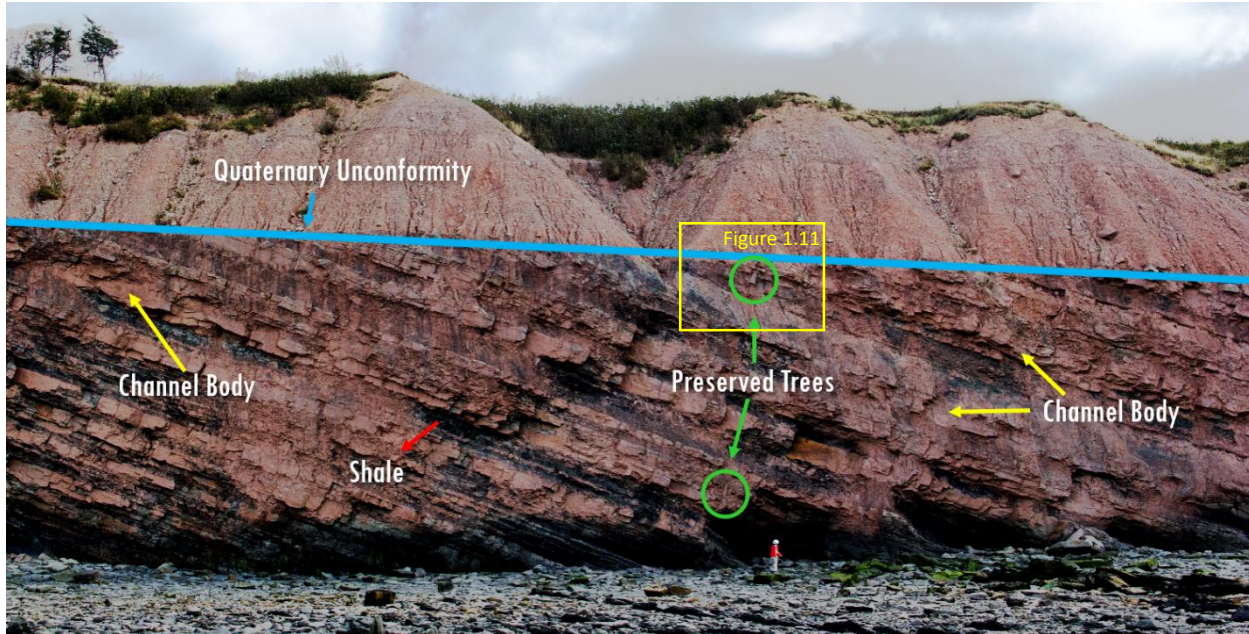


Figure 1.10 – Sedimentary and stratigraphical characteristics of the Joggins Formation at Cole Mine Point. Blue line: Quaternary Unconformity, yellow arrows: channel bodies, red arrow: interbedded shale, green circles: preserved tree.



Figure 1.11- Fossil tree within the Joggins Formation at Coal Mine Point (Cumberland Basin, Nova Scotia).

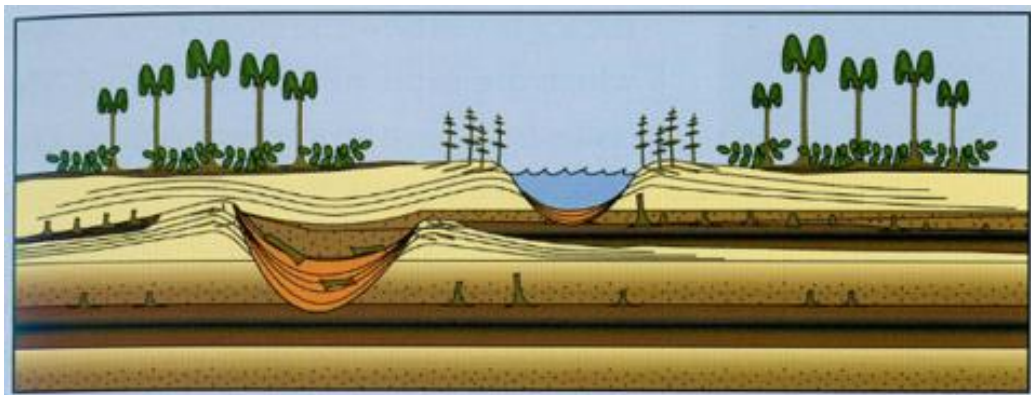


Figure 1.12 – Schematic representation of channel architecture and faunal dynamics during the deposition of the Joggins Formation during the Carboniferous (Cumberland Basin, Nova Scotia) (Fensome & Williams, 2001).

Preservation is cast-and-mold type, and the fossils are very large and representative of the flora during the Carboniferous (Figure 1.13). Some types of fossils found at the outcrop are *Alethopteris*, *Calamites*, *Lepidodendron*, and *Sigillaria* (Calder, 2012). Currently the JFCC maintains a record of the preserved trees by updating a measured section log with all new discoveries.



Figure 1.13 - (A) Cast of a *Calamites* and (B) Mold and cast of a *Sigillaria*.

1.3.3.1.1 *Alethopteris*

Alethopteris are usually seen as imprints within the rock surface. These dark shades imprints are coalified and they resembles modern fern like plants (Figure 1.14).

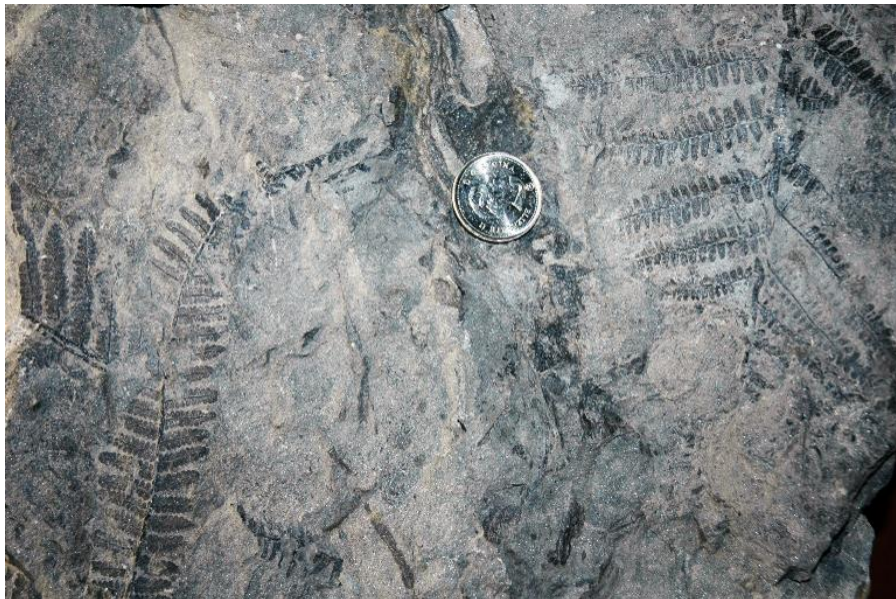


Figure 1.14 - *Alethopteris* coal imprint (dark leaf like shapes) on rock surface, sample from Dalhousie University, Earth Science Department.

1.3.3.1.2 *Calamites*

Calamites are round and elongated shapes, and resemble ancient horsetail weeds. They are estimated to grow up to 10 m tall, probably in small patches before they were entombed by the sediments (Thomas, 2012). They look like modern bamboos (Figure 1.15).



Figure 1.15 - *Calamites* Fossil, sample from Dalhousie University, Earth Science Department.

1.3.3.1.3 *Lepidodendron*

Lepidodendron are one of the tall trunks that are visible at outcrop, and they can be identified by a unique diamond-shape pattern within the bark (Figure 1.16). These trees are a type of lycopod tree and are known to grow up to 30 m tall.



Figure 1.16 - Highlight of diamond shape pattern within the bark of *Lepidodendron*, sample from Dalhousie University, Earth Science Department.

1.3.3.1.4 *Sigillaria*

Sigillaria is also another kind of lycopod tree, and they are known to grow very tall, up to 30 m. They have a unique honeycomb pattern shape, unlike the *Lepidodendron* (Figure 1.17).

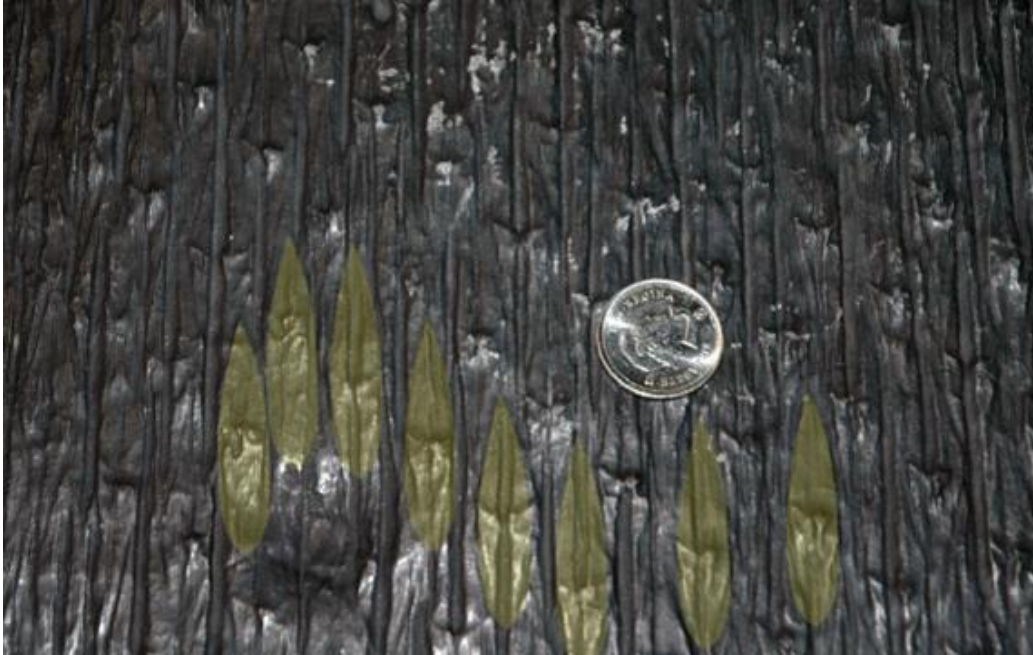


Figure 1.17 - Highlight of honeycomb shape pattern within the bark of *Sigillaria*, sample from Dalhousie University, Earth Science Department.

1.3.4 Meanderbelt Channels

Meandering rivers are one of four end-member types (straight, meandering, braided, and anastomosed) of rivers (Prothero & Schwab, 2004). Most meandering rivers occurs in regions of shallow slope, with a well-developed floodplain. They contain a high ratio of suspension load to bed load material, usually have cohesive bank material, and have a sandy bedload (Reading 1996; Miall 2010). These channels are a result of lateral migration of the fluvial system. In areas of small bending, erosion of the outer bank sediment and subsequent deposition of sediment along the inner bank of the channel occurs (Prothero & Schwab, 2004). The continuous erosion and deposition within the channels creates a steep profile along the outer bend and a gradual profile along the inner bend, creating a non-center maximum depth along the profile (known as the thalawag) (Figure 1.18). The shape of this profile produces maximum flow rates along the thalawag of the channel results in a water flow patterns that are maximum along the thalawag, further facilitating erosion of the outer bank and deposition along the inner bank (Reading 1996; Prothero and Schwab 2004). Meander systems range from coarse gravel channel-lags to very fine grained floodplain deposits. Facies associated with meander channel deposits have been summarized by Miall (2010).

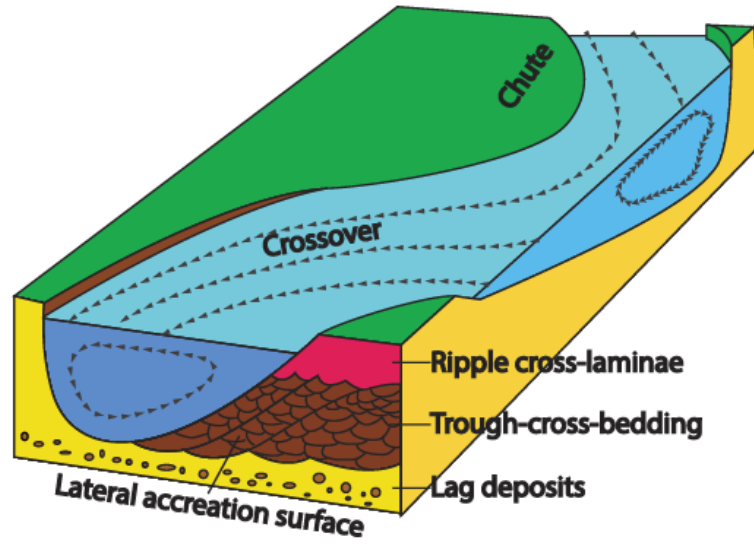


Figure 1.18 - The architecture and flow regime of a meander channel (modified from Prothero & Schwab, 2004).

2 Methods and Data Processing

Data collection was performed using the following survey equipment: Differential Global Positioning System (DGPS), Light Detection and Ranging (lidar), scintillometer, and permeameter. The equipment was provided by the Basin and Research Lab and Patterns Numerical and Analogue Modeling Laboratory (DPGS), Dalhousie University, Earth Sciences Department.

2.1 Differential Global Positioning System (DGPS)

Differential Global Positioning System is an advanced form of GPS for improved location accuracy. This system of GPS surveying consists of two parts: the base station (Figure 2.1) and the mobile rover (Figure 2.2). The fix base station uses its location to calculate the differential position from the satellites receptions and then then apply corrections that are transmitted to the mobile rover, resulting in an accurate positioning points within a few centimeters.



Figure 2.1 – DGPS base station (photo by Trevor Kelly).



Figure 2.2 – DGPS rover.

One of the advantages of utilizing a fix base station-rover configuration is the elimination of the multipath effect (Figure 2.3). The multipath effect is the error (signal disruption) generated by the reflection of satellite signals from solid surfaces, such as buildings, or the cliff where we are trying to perform a survey (National Coordination Office for Space-Based Positioning, Navigation, and Timing, 2014).

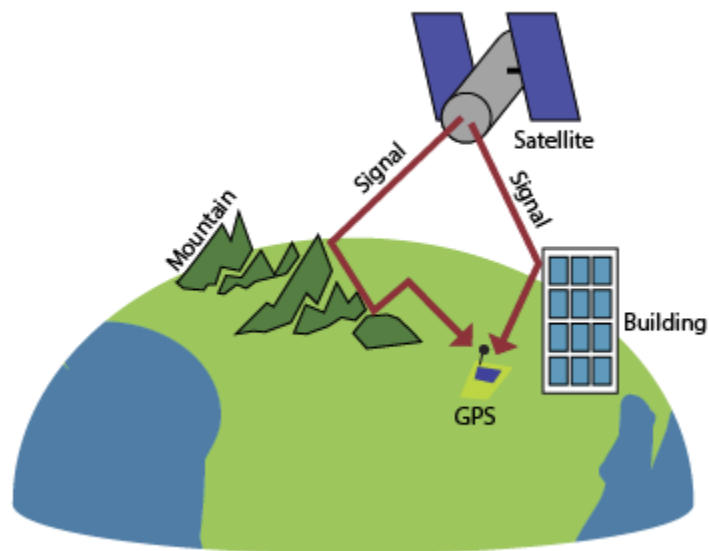


Figure 2.3 - Multipath effect of GPS, creating errors within the GPS device.

The base station was placed over a previously surveyed well-head cap (Rafuse & Wach, 2011) near the Joggins Fossil Cliff Center. The well-head was used as the survey marker for correction of the measurements obtained by the rover. The rover was used to record the location of several targets need for georeferencing the lidar survey. These measurements are required so that the recorded data can be placed in the correct spatial position, so that the multiple lidar surveys can be merged in a 3D model (Figure 2.4).



Figure 2.4 – Targets used for georeferencing. The targets have high reflective background (reflective black) contrasted with a less reflective centre circle, design by Johnathan Thibodeau.

A minimum of three targets are required to correctly georeference each scan. Each target within the survey was placed at a different height and widely spread across the entire area to be scanned to maximize accuracy. If targets are closely spaced or at the same elevation, the accuracy of the survey can be compromised.

2.2 Light Detection and Ranging (lidar)

Lidar utilizes a laser as a light emitting source that can scan an entire outcrop that covers kilometers (Figure 2.5).



Figure 2.5 - Optech in. ILRIS HD lidar on a tripod, performing a scan (photo by Darragh O'Connor).

This lidar records at a speed of ten thousands of points per second, each point is recorded by the lidar in real-time. Each point is calculated by measuring the time interval between laser pulses that leaves and returns to the scanner (Equation 2.1). In addition to special coordinates a fourth dimension, intensity, is also recorded. The intensity property corresponds to the intensity of the reflected laser pulse which depends on the lithology of the surface reflecting the beam (Figure 2.6). Once the complete scan is performed, the lidar will have a very dense spatial dataset. This collected data points, is a high resolution and representation of the surface scanned, and is referred to as Point Cloud Data. This Point Cloud Data (PCD) can be utilized for processing and generation of Digital Outcrop Models (DOM). This DOM can be used to study the rock properties of the outcrop.

Equation 2.1,

$$\text{Range} = \frac{ct}{2}$$

Equation 2.1 - Equation of Range distance calculation that the lidar performs while scanning.

t: Time interval between sending/receiving the pulse (ns)

c: speed of light (0.2998 m/ns)

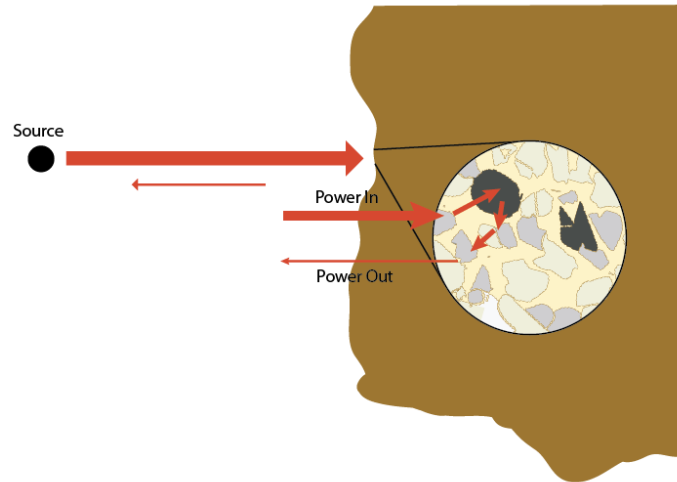


Figure 2.6 - The intensity property corresponds to the intensity of the reflected laser pulse which depends on the lithology of the surface reflecting the beam. A laser pulse is emitted from the source towards the outcrop. As the pulse reflects from the outcrop it returns back to the source. During the reflection some intensity of the pulse is lost (after Burton, et al., 2011).

The lidar used in this survey is the Optech Inc. ILRIS HD lidar, which uses a laser rated at Class 1. The lidar was placed about 45 m away from the cliff and the 3 georeferencing targets were placed along the cliff at different elevations. The locations of the lidar and the targets were capture using the DGPS. The lidar scanned 235 m of the cliff using the following settings: resolution of 15 mm and four individual scans to cover the survey area (Figure 2.7). With the acquisition of the data the scanner also takes a digital photograph of the area that it scans as a photographic reference.



Figure 2.7 – Photomontage depicting the Coal Mine Point study area taken from the intertidal zone by the lidar. The lidar scanned a total of four segments for this section and for each segment a digital photograph is recorded. The four photographs are compiled here.

Positioning the lidar in the ideal location to perform the survey is critical, in order to obtain the most optimal data quality for analysis. The lidar has an ability to rotate 360° horizontally and a field of view of 40° horizontal x 40° vertical. The area of interest must be able to fit within this scan-frame. This ILRIS HD lidar has a minimum of 20 μ-radians as a rotational movement between each laser impulse. For a more detailed scan, the device needs to be close to the target, although being close may cause an

ineffective scan. The minimum working range for this scanner is 3 m. At greater distances from the target, the wider the angle each laser pulse becomes (Figure 2.8), resulting in a decrease in image resolution.

Maximizing the field of view of the scan is optimal for the avoidance of areas that cannot be scanned due to obstructions of objects, such as overhangs of the cliff obstructing the path of the laser pulse (shadow zones) (Figure 2.9). This can be corrected by repositioning the lidar scan in another angle and performing a separate scan. Merging these separate scans allow to reconstruct the entire cliff face, with minimal or no shadow zones. In order to merge the scans together, the georeferencing targets (Figure 2.4) were used to facilitate this process. Each georeferencing target has a very high reflective background, so it is easily found and identified when we are georeferencing the data set in ArcGIS.

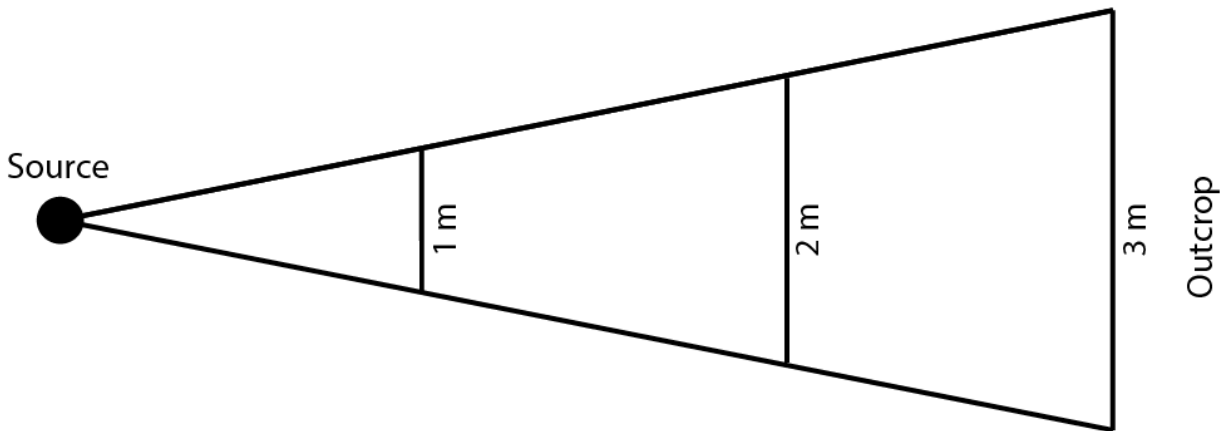


Figure 2.8 - Angle of dispersion of laser beam. As the laser pulse source is at a further distance from the outcrop, the horizontal distance between each laser pulse increases, in turn reducing the image resolution.

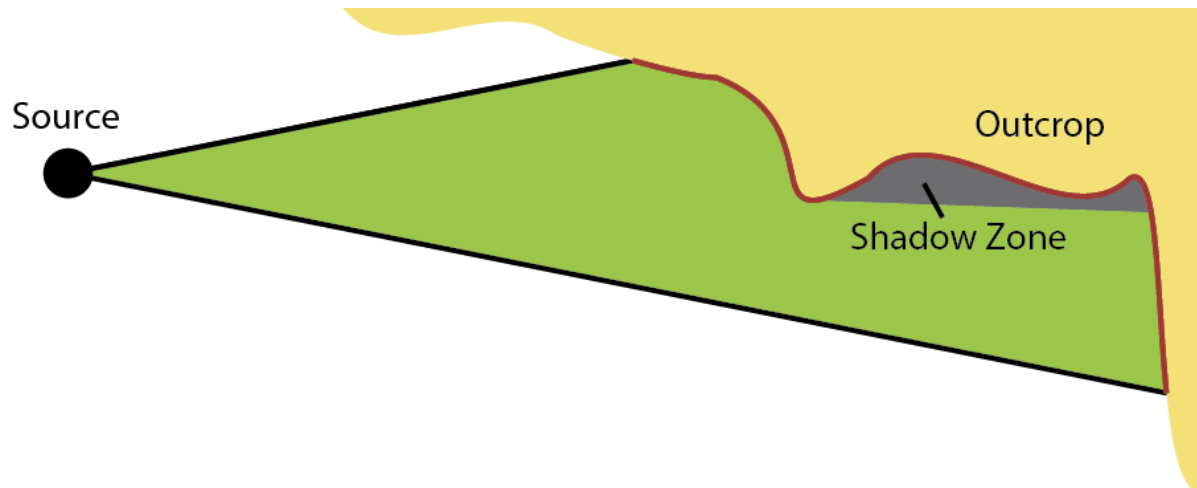


Figure 2.9 – An example of a shadow zone. An overhang is obstructing the path of the laser pulse. Resulting in an area with no data. The red line is the intended area of capture along the outcrop. The grey area is the portion of the outcrop where no data are collected.

2.3 Scintillometer

The scintillometer (Figure 2.10) is a handheld device that measures the natural radioactivity of rocks. The scintillometer/gamma-ray spectrometer used in this project is an Exploranium GR-130. The scintillometer contains a glass vial as part of the internal structure, which is sensitive to temperature and humidity, affecting the accuracy and precision of measurements, therefore calibration using a cesium-137 chip is required to ensure the accuracy of the data collected.



Figure 2.10 - Handheld Scintillometer, it measures the spectral gamma emission of the formation (K, U, Th)

2.4 Permeameter

Permeability is a parameter indicating the ability for fluids or hydrocarbons to flow through a rock (Figure 2.11 – Schematic representation of permeability.). The handheld permeameter used in this survey was a TinyPerm II, made by New England Research Inc. (Figure 2.12). This pneumatic device is portable and utilizes a pump handle to compress air into the chamber. As the air escapes from the nozzle into the rock, the permeameter records the rate the air enters the rock, and this can be used as a proxy for rock permeability. These measurements are converted to Darcy scale using the calibration provided by the manufacturer (Figure 2.13). Permeability is a measurement of the capacity of a rock to allow fluids to flow through it, i.e. Darcy's Law. The standard unit for permeability is m^2 , however in Earth Sciences is commonly used the Darcy (D), in which $1D \approx 10^{-12}m^2$. To collect these data, the permeameter was held onto the surface of the rock for 60-120 seconds depending upon the lithology to measure the volume of air that passes through the lithofacies. Permeability measurements were taken on clean surfaces from rock samples collected.

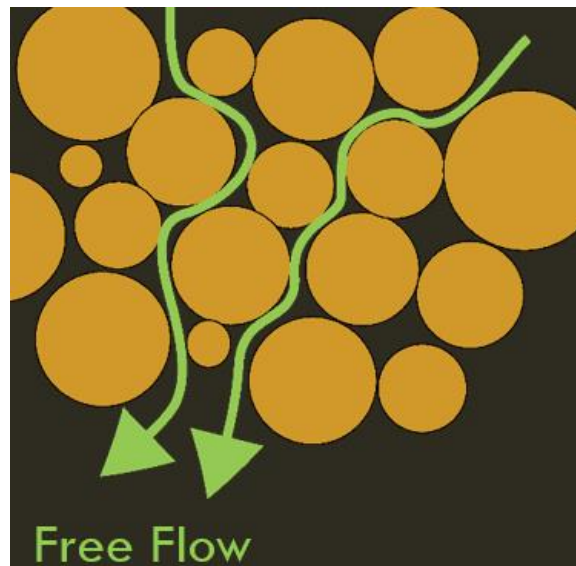


Figure 2.11 – Schematic representation of permeability.



Figure 2.12 – Pneumatic device to measure permeability of the rock, in mD this is a TinyPerm II by New England Research Inc.

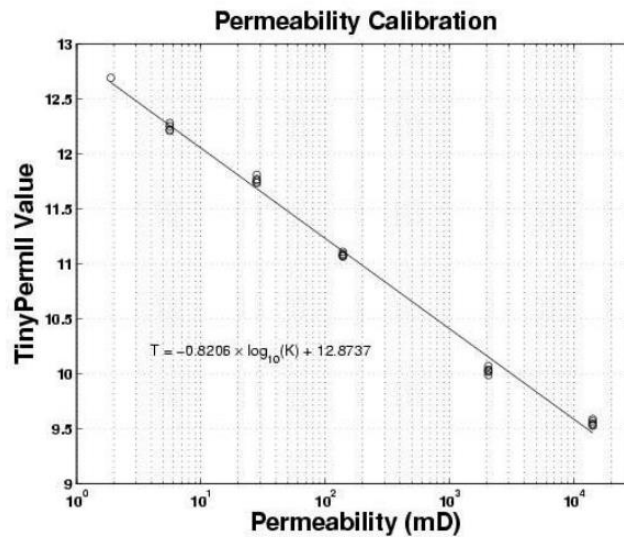


Figure 2.13 - TinyPerm II Permeability Calibration Graph. T: TinyPerm II reading K: Permeability Value (mD) (New England Research Inc., n.d.).

2.5 Data Processing

2.5.1 ArcGIS

ArcGIS is a Geographic Information System (GIS) software used to georeference the PCD collected by the lidar. To georeference the data set, the data was loaded into ArcScene, a sub-program within ArcGIS. A comma-separated values (CSV) file containing the collected data was imported into ArcScene. Each georeferencing target was matched to the centermost point of the target with the coordinates recorded by the DGPS. Once the operator was satisfied with the data in 3D by ArcScene, ArcGIS was used to georeference the points to the correct spatial location. The final file was in CSV format.

In ArcGIS, the CSV file was loaded to create a shapefile. This process is very computational intensive due to the amount of data points recorded by the lidar. Points that are not part of the outcrop,

such as the intertidal zone and vegetation at the top of the cliff, were deleted from the shapefile. This filtration and reduction of points was needed to help computational process of the entire data set. The original data set included about nine million points and was reduced to six million points. Once the amount of data points deleted was satisfactory, the file was saved as a shapefile and exported as a CSV file to be imported into Petrel.

2.5.2 Petrel

Petrel is a Schlumberger software product intended for modeling, interpretation and simulation of digital geological data. As previously discussed, intensity of the laser pulse depends on the composition of the reflecting surface: quartz-rich sandstones will have higher reflectivity values and clay-rich shale will have lower reflectivity values (Burton, et al., 2011) (Figure 2.14). Other studies also indicates that different units can be identified by utilizing the intensity of a lidar scan (Hartzell, et al., 2014), although different calibration has to be done per outcrop scan (Campos, et al., 2013). Petrel is a powerful application for building models, interpretation and simulation of subsurface, but for this project we had limitations for this type of application, such as generating a surface from PCD. Other studies utilize other type of 3D modeling software, like GOCAD and Polyworks (Bellian, et al., 2005; Buckley, et al., 2013).

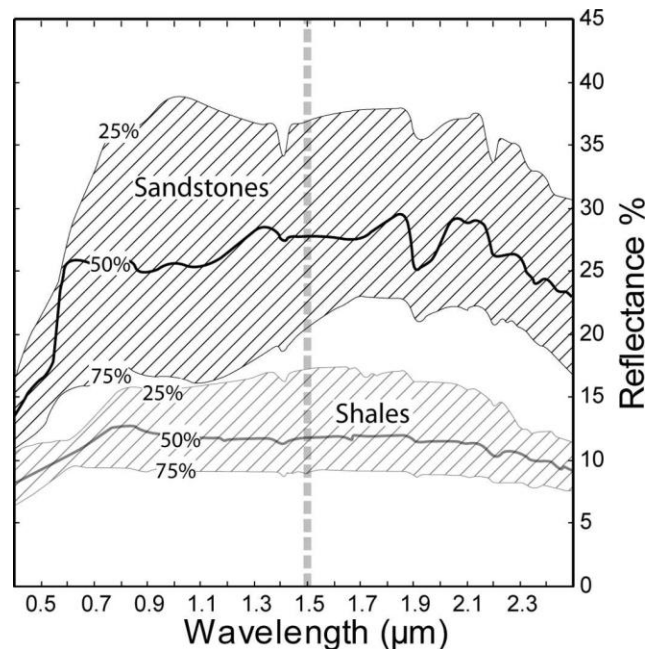


Figure 2.14 - NASA JPL library spectroscopy (Baldridge, et al. 2008 cited in Burton, et al. 2011), solid sample data showing median (solid line) and quartiles (dashed lines) for shale (gray) and sandstone (black). The dashed line is the approximate wavelength of terrestrial lidar. Note the spectral separability between sandstones and shale at different wavelengths.

3 Results

3.1 Differential Global Positioning System (DGPS)

Using the DGPS is used to provide high precision coordinates in three dimensions to reference the targets (Table 3.1 Table 3.4).

Table 3.1 – Location of the lidar setup near Coal Mine Point.

Point ID:	CMP_1		
Description:	Location of the lidar setup near Coal Mine Point		
Class:	MEAS		
Subclass:	GPS Fixed		
3D CQ:	0.023 m		
WGS84 Lat:	45°41'57.87993" N	Easting:	386,962.38 m
WGS84 Long:	64°27'07.14929" W	Northing:	5,061,676.07 m
WGS84 Ell Ht:	-1.240 m		
Time:	12:26:32 PM		
Date:	31.05.13 (D.M.Y)		
Instrument:	GPS		
Source:	Survey (Static)		
Coordinates:	X = 1,924,440.421 m		
	Y = - 4,025,987.253 m		
	Z = 4,541,975.203 m		

Table 3.2 - Location of the left georeferencing Target 1 as viewing the cliff face from the water.

Point ID: CMP_1_T1			
Description:	Location of the left georeferencing Target 1 as viewing the cliff face from the water		
Class:	MEAS		
Subclass:	GPS Fixed		
3D CQ:	0.026 m		
WGS84 Lat:	45°41'58.86683" N	Easting:	387,069.97 m
WGS84 Long:	64°27'02.19604" W	Northing:	5,061,704.58 m
WGS84 Ell Ht:	3.875 m		
Time:	12:23:37 PM		
Date:	31.05.13 (D.M.Y)		
Instrument:	GPS		
Source:	Survey (Static)		
Coordinates:	X = 1,924,529.237 m		
	Y = - 4,025,924.587 m		
	Z = 4,542,000.144 m		

Table 3.3 - Location of the georeferencing Target 2 as viewing the cliff face from the water.

Point ID: Georeferencing Target 2			
Description:	Location of the georeferencing Target 2 as viewing the cliff face from the water		
Class:	MEAS		
Subclass:	GPS Fixed		
3D CQ:	0.023 m		
WGS84 Lat:	45°41'56.98459" N	Easting:	387,039.72 m
WGS84 Long:	64°27'03.55149" W	Northing:	5,061,647.03 m
WGS84 Ell Ht:	3.055 m		
Time:	12:22:05 PM		
Date:	31.05.13 (D.M.Y)		
Instrument:	GPS		
Source:	Survey (Static)		
Coordinates:	X = 1,924,520.471 m		
	Y = - 4,025,974.240 m		
	Z = 4,541,958.970 m		

Table 3.4 - Location of the georeferencing Target 3 as viewing the cliff face from the water.

Point ID:	Georeferencing Target 3		
Description:	Location of the georeferencing Target 3 as viewing the cliff face from the water		
Class:	MEAS		
Subclass:	GPS Fixed		
3D CQ:	0.016 m		
WGS84 Lat:	45°41'56.58706" N	Easting:	386,989.33 m
WGS84 Long:	64°27'05.86754" W	Northing:	5,061,635.67 m
WGS84 Ell Ht:	1.036 m		
Time:	12:20:40 PM		
Date:	31.05.13 (D.M.Y)		
Instrument:	GPS		
Source:	Survey (Static)		
Coordinates:	X = 1,924,478.445 m		
	Y = - 4,026,002.502 m		
	Z = 4,541,948.953 m		

3.2 Light Detection and Ranging (lidar)

The final scan contains nine millions of data points recorded by the lidar and stored in a RAW format. This RAW format contains all the data collected by the scanner and can only be read by the software provided by the manufacturer of the lidar. We used the parsing software provided by Optech Inc. for the ILRIS HD lidar to decode this RAW format into a format that is readable by ArcGIS and Petrel. The parser software can convert the data into multiple formats, but for our study we saved it as a XYZ format file. This file format has the X, Y, Z and intensity values for each point recorded after being parsed, which translated the data points recorded by the lidar, into an ASCII file type XYZ (Figure 3.1).

```

833963.693 9999948.000 1.647 58
833963.631 9999948.000 1.650 104
833963.631 9999948.000 1.646 79
833963.631 9999948.000 1.650 75
833963.568 9999948.000 1.650 82
833963.568 9999948.000 1.652 87
833963.568 9999948.000 1.652 88
833963.568 9999948.000 1.652 86
833963.506 9999948.000 1.654 74
833963.506 9999948.000 1.655 66

```

Figure 3.1 - File format of an XYZ output from Optech Inc. parser, based on data collected for this study.

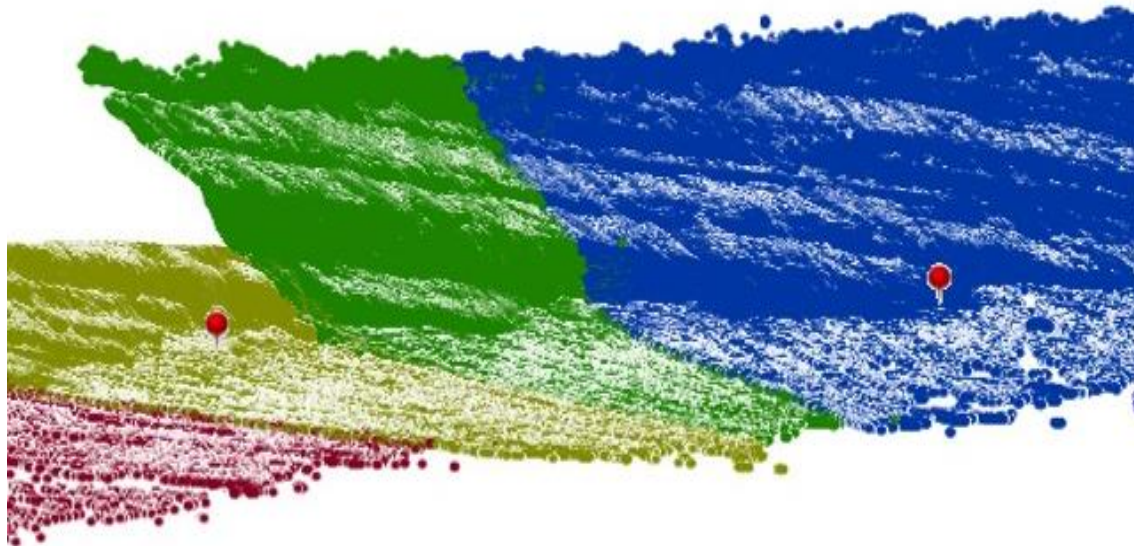


Figure 3.2 – Unprocessed lidar scan after import into ArcScene. Each colour represents a different scan section; 4 sections total. Red pins indicate the location of the georeference targets in the scan.

3.3 Scintillometer

Gamma-ray values were recorded along the base of the outcrop at Coal Mine Point, with five measurements per stop along the outcrop (Figure 3.3). Using the mean of value of these measurement from each stop, a pseudo gamma ray log was constructed (Figure 3.4). This is a technique currently used to study correlation of well log produced at outcrop from a handheld gamma-ray (Slatt, Jordan, & D'Agostino, 1992). Figure 3.4 shows that the higher values of gamma ray are associated with shale (and rare coal), and lower values are associated with the sand bodies. Correlating the pseudo gamma ray log with previous stratigraphic section by Davis (2005), the relationship of the sand bodies (lower cps) and shale layers (higher cps) with this pseudo gamma ray log is apparent (Figure 3.4).



Station	Relative Position	Scintillometer Measurement (counts per second)					Avg	Notes (descriptions by G. Wach with assistance from C. Dickson)
		1	2	3	4	5		
001	0	170	165	172	160	163	166	host sandstone with shale rip-up clasts; fine to medium-grained sandstone; angular to subangular clasts (up to 4cm)
002	16	180	183	176	187	184	182	fine to lower-medium-grained sandstone
003	21	250	249	246	252	250	249.4	grey; silty sandstone; beeped - U present; small, blocky, fissile
004	31	212	221	227	225	223	221.6	siltstone; massive
005	44	198	199	207	199	211	202.8	very fine-grained sandy siltstone
006	50	158	165	161	169	155	161.6	current rippled sandstone; trace fossils on surface
007	61	220	221	219	235	226	224.2	slightly sandy siltstone with iron-pyrite nodules (up to 5cm)
008	67	203	192	207	195	195	198.4	fine to lower-medium-grained sandstone
009	100	228	238	232	227	230	231	red to grey interbedded siltstone
010	107	187	197	189	191	181	189	parallel laminated fine-grained sandstone; some ripples; slightly silty
011	121	217	205	208	212	210	210.4	red to grey very-fine grained sandstone; current ripples
012	133	244	256	253	238	241	246.4	dark grey; small blocky; silty clay
013	152	202	197	208	200	204	202.2	silty very-fine-grained sandstone
014	161	221	237	226	235	216	227	small, blocky, sandy siltstone
015	196	249	251	257	262	257	255.2	medium-grained; small blocky; silty clay sandstone
016	198	184	178	185	185	182	182.8	very-fine-grained to fine-grained sandstone with 30-50cm beds; capped with small 1x5m channels; tree removed by JFCC
017	217	219	236	225	218	212	222	red claystone
018	224	202	198	203	215	196	202.8	intershale - 10cm thick *note station 015, 016, & 017 form a channel body*
019	227	177	178	182	183	184	180.8	sandstone
020	249	230	235	237	240	234	235.2	medium-grained; grey; silty clay; blocky
021	257	209	202	213	217	214	211	coal; 15cm
022	259	203	212	208	200	201	204.8	fine-grained sandstone with fine-laminations of grey-silty claystone (cm scale)
023	400	94	99	102	93	98	97.2	massive sandstone
024	401	96	82	88	98	99	92.6	cross-trough; thin beds; sandstone
025	402	90	92	103	97	110	98.4	massive sandstone

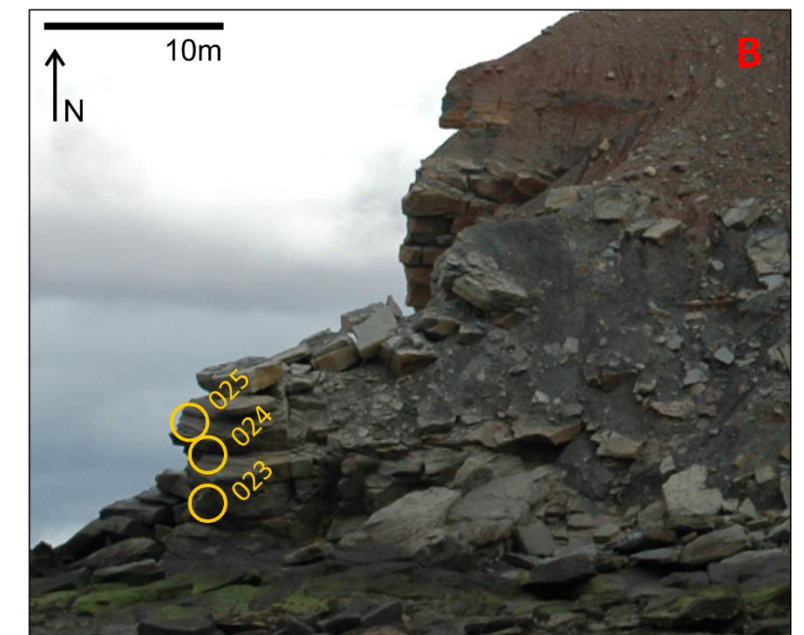


Figure 3.3 - Scintillometer measurements of the Joggins Formation at Coal Mine Point section. Figures A and B.

Table 3.5 – Scintillometer measurements collected at Coal Mine Point with corresponding lithological descriptions.

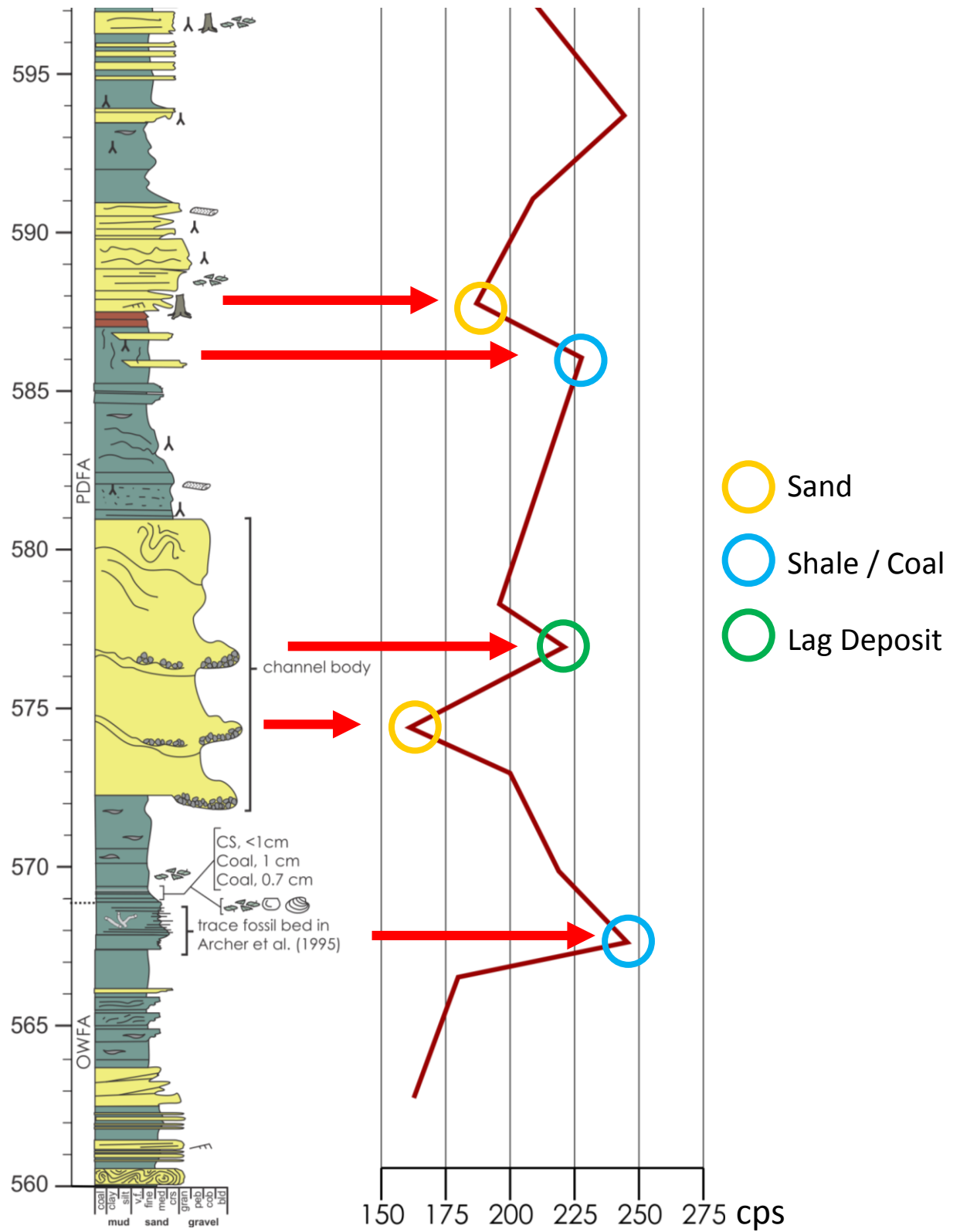


Figure 3.4 – Correlation of pseudo gamma-ray with the measured stratigraphic section of the Joggins Formation at Coal Mine Point (stratigraphical section from Rygel, 2005). Gamma Ray is representative of the lithology.

3.4 Permeameter

Permeability was measured in several samples collected around the base of the outcrop. Measurements were performed in hand specimens instead of outcrop, due to the hazard of falling rocks at the CMP. Permeability measured from the hand samples ranged from 66 mD to 1917 mD (Table 3.6). These samples present good to excellent permeability (Table 3.7) (Nebaway, Rochette, & Geraud, 2009), indicating that these sandstones have a good to excellent storage capacity for fluids. Fractures on the rock can impact the fluids flow, increasing the permeability of the rock.

Permeability data (Table 3.6) indicates that all samples range from good to excellent permeability ranking. All samples, with the exception of sample 4, correspond to medium-grained sandstone. Sample 4, classified as a coal, has very good permeability values due to fracturing.

Table 3.6 - Permeability measurements of Coal Mine Point and its ranking according to Table 3.7.

Sample	Lithology	Reading	Perm. (mD)	Ranking
1	sandstone	10.64	527	Very Good
2	sandstone	11.38	66	Good
3	sandstone	10.86	284	Very Good
4	coal	10.75	387	Very Good
5	limestone	10.33	1,258	Excellent
6	sandstone	10.44	924	Very Good
7	sandstone	10.18	1,917	Excellent
8	sandstone	10.88	269	Very Good

Table 3.7 - Ranking of Permeability (K) (Nebaway, Rochette, & Geraud, 2009).

Range	Rank
$1 < K \leq 10$ mD	Fair
$10 < K \leq 100$ mD	Good
$100 < K \leq 1000$ mD	Very Good
$1000 < K$	Excellent

3.4.1 Hand Samples

Sample 1:	GW101-2013TK		
Rock type:	Sandstone	Permeability (mD):	527
Colour:	Light grey		
Grain:	Equigranular and medium grains		
Fragments:	Black needle like shape rock fragments		
HCl:	Reacts vigorously, suggest to have carbonate components		



Sample 2:

GW102-2013TK

Rock type:	Sandstone	Permeability (mD):	66
Colour:	Light Grey		
Grain:	Equigranular and medium grains		
HCl:	Reacts weakly, suggest to have carbonate components		



Sample 3:

GW103-2013TK

Rock type:	Clastic Sandstone	Permeability (mD):	284
Colour:	Grey		
Grain:	Equigranular and medium grains		
HCl:	Reacts weakly, suggest to have carbonate components		



Sample 4:

GW104-2013TK

Rock type:	Carbonaceous Coal	Permeability (mD):	387
Colour:	Sub-vitreous		
Other:	Massive, Homogenous and non-clastic		
	Very Light		
HCl:	Presence of calcite within veinlets throughout the sample, probably formed during secondary mineralization by calcite precipitation when the coal was fractured		



Sample 5:

GW105-2013TK

Rock type:	Limestone	Permeability (mD):	1,258
Colour:	Medium to Dark Grey		
Grain:	Fine to very fine grained		
Feature:	Ellipsoidal shaped features, possible representing fossils or fossil fragments occurring throughout the sample		
HCl:	Reacts vigorously		



Sample 6:

GW106-2013TK

Rock type:	Clastic Sandstone	Permeability (mD):	924
Colour:	Light Gray		
Grain:	Equigranular and medium grains		
HCl:	Reacts weakly, suggest to have carbonate components		



Sample 7:

GW107-2013TK

Rock type:	Clastic Sandstone	Permeability (mD):	1917
Colour:	Light Grey		
Grain:	Equigranular and medium grains		
HCl:	Reacts, suggest to have carbonate components		



Sample 8:

GW108-2013TK

Rock type:	Sandstone	Permeability (mD):	269
Colour:	Light Grey		
Grain:	Equigranular and medium grains		
Fragments:	Lithic fragment about 10 mm long and 5 mm wide (Dark Colour)		
HCl:	Reacts moderately, suggests carbonate components		



3.5 Petrel

As previously mentioned (2.5.2), using intensity for classifying rocks separate the sandstones from the shale/coal intervals of the Joggins Formation at Coal Mine Point section. Adjusting the colour level of the values of intensity allows the operator to see the areas of higher values of intensity recorded by the lidar, indicating high reflection. It is possible to differentiate the sandstones from the shales at CMP. The model illustrates the CMP outcrop and the intensity values of the PCD, displaying how intensity can be used as a proxy for classifying lithology (Figure 3.5). In Figure 3.5 the sandstone beds correspond to higher intensity values, with some high intensity values visible in the top of the section, most likely due to vegetation and mine tailing (Figure 3.6). These mine tailings comprising sandstone and siltstone were the result from production of coal in the region, as Joggins was known as a coal mine producing area.

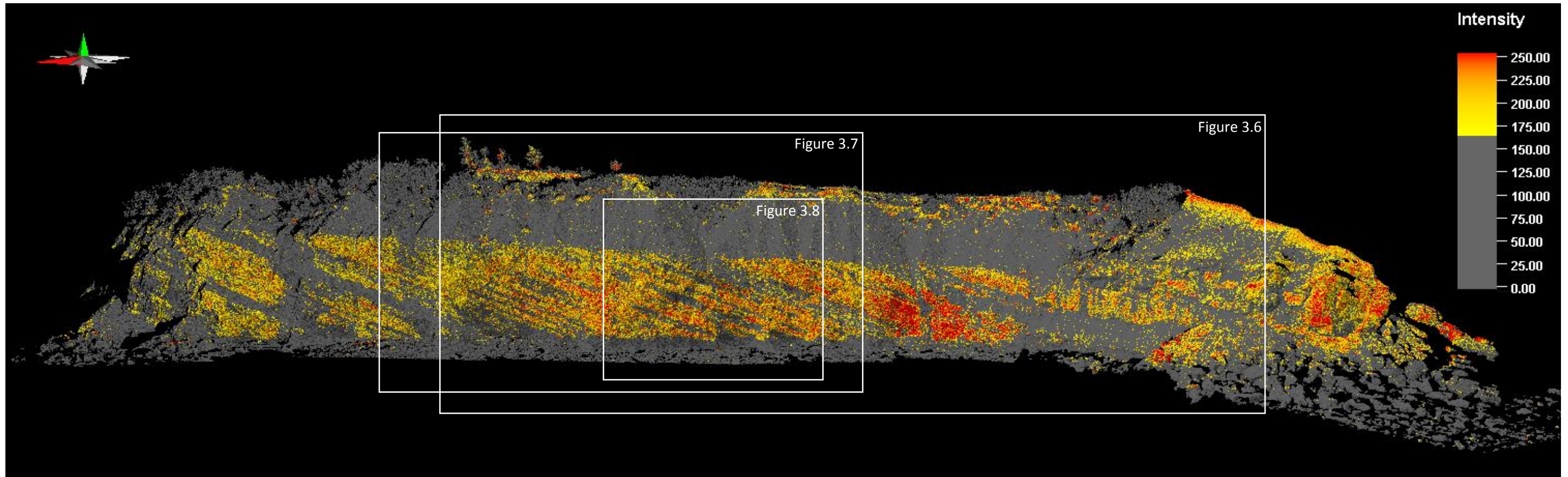


Figure 3.5 - Petrel render of the data set. The warmer yellow and red hues indicates higher intensity values due to the greater reflectivity of the quartz component in the sandstones Red arrow indicates north and the horizontal distance.

A very distinctive horizontal gray top (low intensity) corresponds to the Quaternary angular unconformity and related sediments such as glacial till with fine grain shale, with cobbles and small boulders that give the high intensity points (Figure 3.6), truncating the Joggins Formation. In these define, thin layers of shale can be seen between the reflective layers of sandstone (Figure 3.7). Mine tailings are predominant in this area because Joggins was a coal mining region in the past. Other factors to take into consideration is the vegetation, as it is also recorded as high intensity.

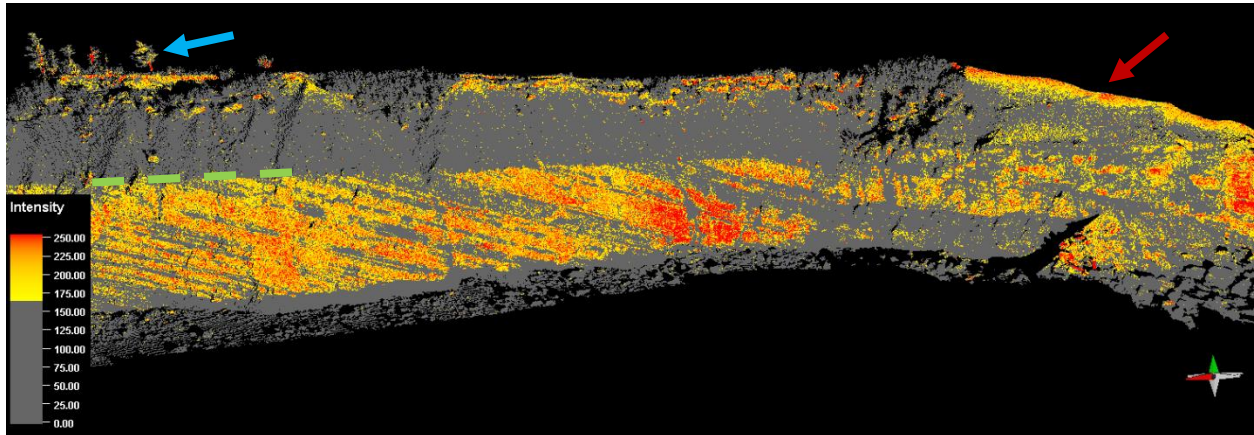


Figure 3.6 – Petrel render image of the data set. Quaternary Unconformity (green dash line), mine tailings (red arrow) and vegetation (blue arrow).

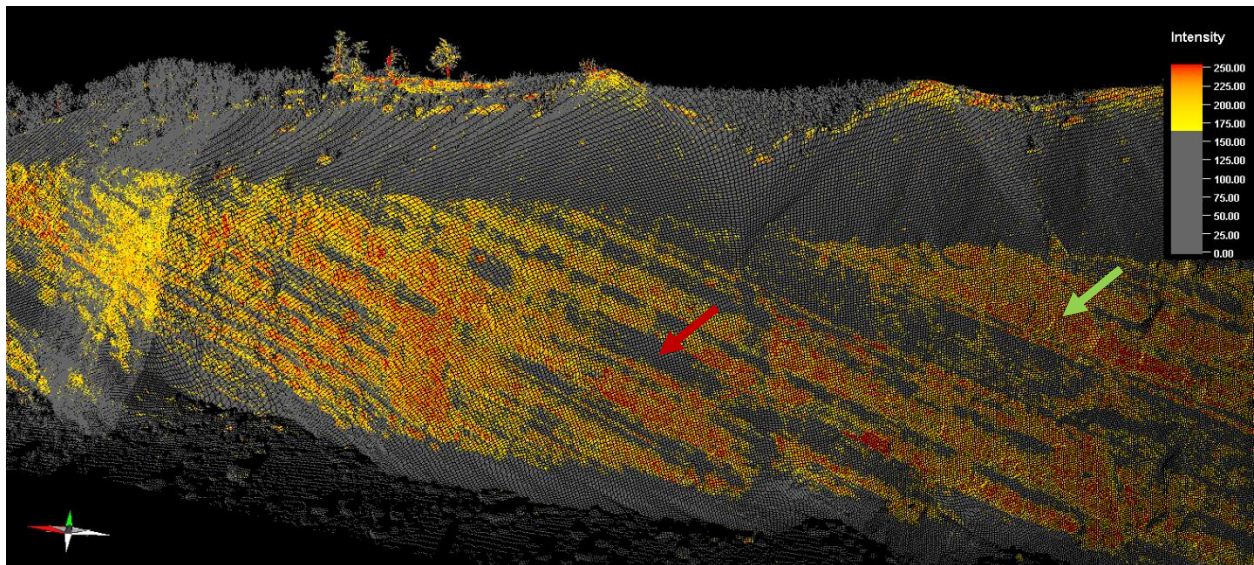


Figure 3.7 - Petrel render image of the data set. Where is possible to identify shales (baffle and barriers, red arrow) and sandstones (reservoirs, green arrow). Reflective intensity differences indicates shales. These shales form barriers or baffles to fluid flow between the sandbodies which are the high reflective images.

Looking at the DOM of the outcrop we can identify some cylindrical shape bodies that we identify at outcrop as preserved tree trunks (Figure 3.8).

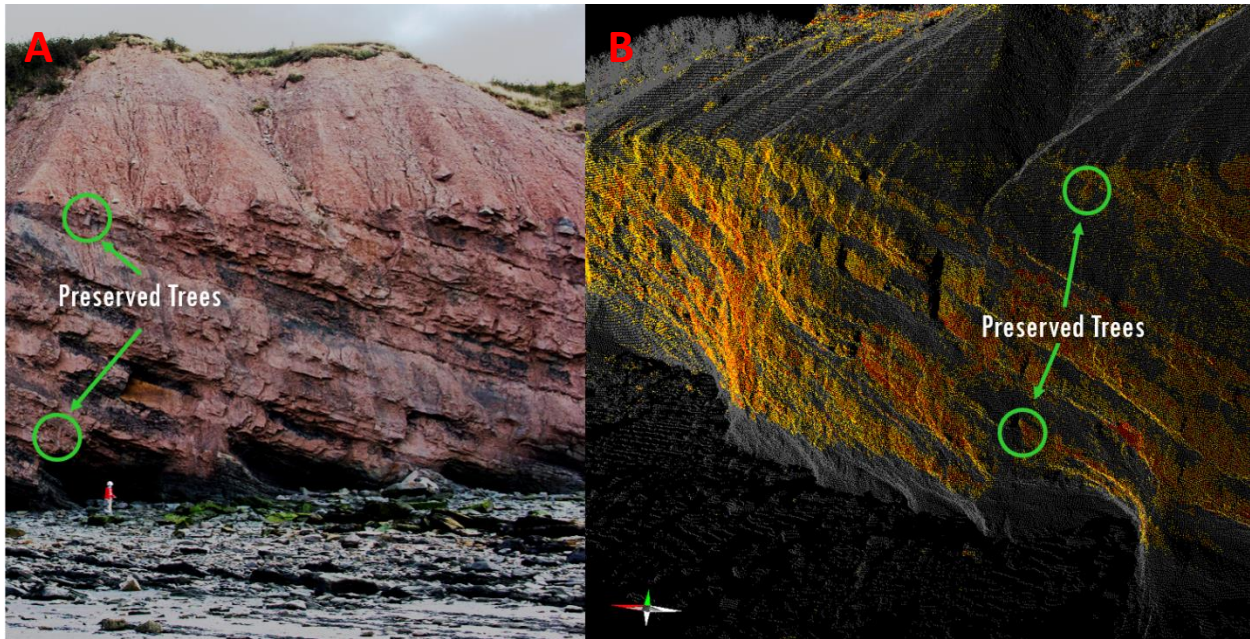


Figure 3.8 - (A) Fossil trees within succession of sediments in a digital photograph. (B) The same fossil trees within the DOM of these same successions. For closer view of preserved tree see Figure 1.11.

4 Discussion

4.1 Light Detection and Ranging (lidar)

4.1.1 Digital Outcrop Model (DOM)

The DOM is a detailed representation of the Joggins Formation at CMP. Using lidar and DGPS, PCD was collected and later spatially georeferenced. Optimizing the field of view (positioning) is very important for collecting data to be used in the DOM. As in Figure 2.9, the positioning of the lidar vs. the outcrop created areas of low reflectivity and shadow zones (Figure 4.1 & Figure 4.2). To correct the low reflective areas and the shadow zones, it is necessary to take several scans of the outcrop from different angles of view. By doing this, the once poorly reflective zones would now have been scanned multiple times and will have a better collection sample of acquired data. Weather conditions must also be taken into consideration when scanning too. During periods of light to heavy precipitation, single drops of rain can cause the diffraction of the laser beam, resulting in misfires and no return signal. This heavily reduces the quality of the collected data and can miss represent the outcrop in the DOM. A previous attempt to scan the outcrop was not successful due to intense precipitation. Reflection and diffraction of the laser pulse by the rain drops substantially decreased the quality of the lidar data. This scan was discarded and not used for this study.

4.1.2 Fossil Tree Identification in DOM

The occurrence of fossilized trees in the study area is well visible in outcrop. Within the DOM, the presence of the fossilized trees is less apparent. In the DOM, the fossilized trees have reflectivity intensities similar to that of sandstones (which will be discussed in more detail in the next section). This makes any fossilized trees within sandstone successions near impossible to identify. If the fossilized trees are within finer grained shale successions, they become much more evident due to the contrasting nature of the reflectivity intensities between the tree and surrounding shale. However, due to the nature of the capturing technique in lidar, the reflectivity of certain lithological successions can be “masked” by a burst of high or low intensity (discussed in 4.1.3). To aid in the identification of fossilized trees, it is necessary to cross reference with a digital photograph. Although the DOM can contain very high resolution of the surface of the outcrop, the geometry of a tree stump can be difficult to see without the aid of a digital photography and measure sections within the outcrop.

4.1.3 Lithological Identification

The intensity recorded by the lidar is useful for investigating outcrop characteristics, depositional patterns, and lithological units (Figure 2.6). Intensity is commonly used in remote sensing for surface evaluations such as, forestry, canyon, topology and others (Burton & Wood, 2010). Previous work has been done utilizing lidar: as a method to develop stratigraphical digital models (Bellian, et al., 2005), rock identification (Campos, et al., 2013), and monitoring coastal erosion (Hobbs, et al., 2010).

At CMP it is possible to observe that the high intensity values corresponds to the quartz-rich sandbodies, while the low intensity values correspond to the more argillaceous lithofacies. In addition it allows to highlight several other sedimentological features, such as discontinuities, channel architecture. The main issue with the use of intensity in the lithological discrimination of the studied section is related with the sensitivity of this parameter to outcrop conservation and wetness conditions, relative orientation between lidar and outcrop, outcrop geometry (vertical and horizontal profile), surface smoothness and intensity cut-off values in the DOM projection.

In the study area, a single survey position was used. This, coupled with the large scale outcrop irregular geometry, resulted in higher and lower intensity values in some areas of the survey, clearly associated with major breaks in the outcrop geometry. Concave geometries (Figure 4.1) resulted in increased intensities, while small promontories (Figure 4.2) promote scatter and resulted in lower intensities.

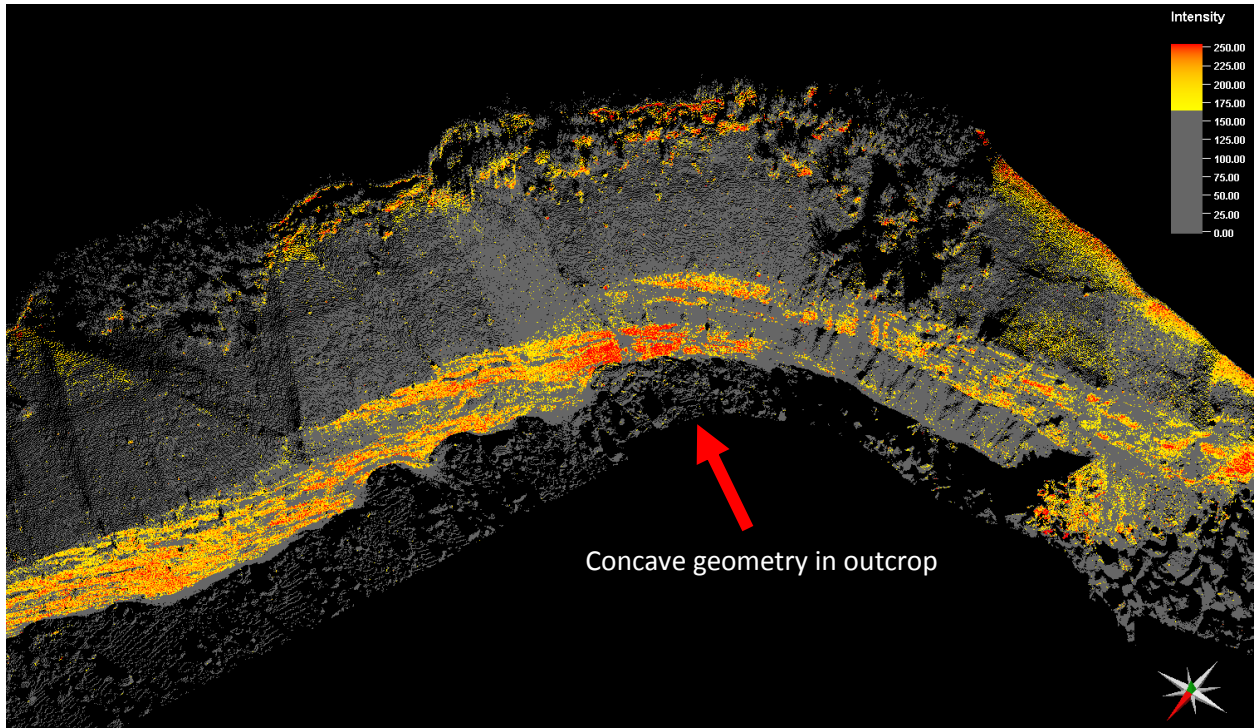


Figure 4.1 - Petrel render image of the data set, showing a concave geometry (red arrow) in outcrop. The concave shape acts as an amplifier of the laser pulse, resulting in higher intensities within the concave shape. This is noted by the warmer red colours.

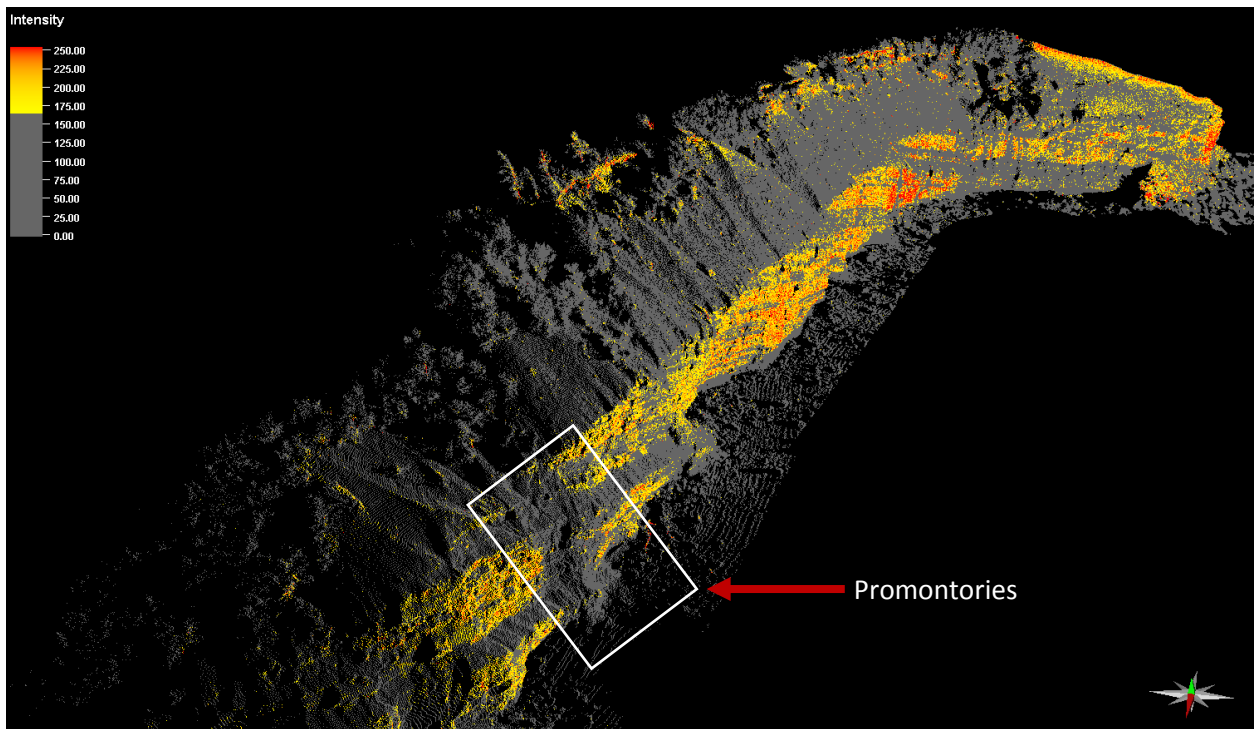


Figure 4.2 - Petrel render image of the data set, showing small promontories (inside white box) in outcrop. The promontories deflect the laser pulse, resulting in lower intensities within the promontory shape. This is noted by the grey colours.

It is possible to observe several areas which have high intensity values. These areas give false appearance of the rock lithology, which gives the appearance that sandbodies are connected. When in reality these sandbodies are not connected (Figure 4.3). In this case, intensity data seems to be conditioned by lidar acquisition and outcrop geometry (Figure 4.3(A)) and surface smoothness (Figure 4.3(B)).

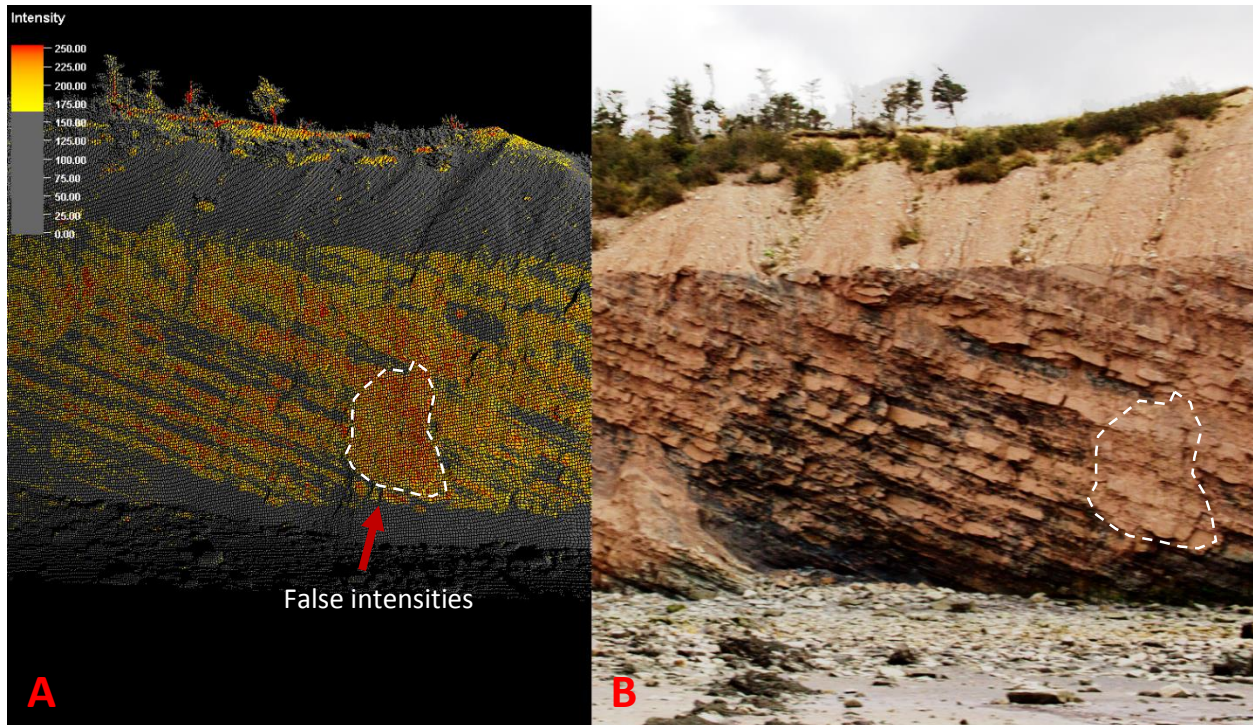


Figure 4.3 - (A) Petrel render of the data set depicting connected sandbodies (Warm red and yellow colours). (B) Digital Photograph of outcrop showing non-connected sandbodies. Dashed line represents the false intensity error that the lidar has recorded.

4.2 Gamma-ray and permeability

The gamma ray log was introduced in the late 1930s and it was the first nuclear tool used to log a well (Schlumberger, 2014). It is commonly utilized in exploration by the oil and gas industry during the drilling of wells and logging of the formations as drilling advances downwards. Gamma ray log measures the natural emission of gamma rays by a given rock unit. They are helpful because they can be used to differentiate low from high radioactive lithologies. High gamma-ray cps usually correspond to organic-rich, argillaceous or carbonated lithologies (coals, shales, marls, and limestones) or U-, Th-, and K-rich minerals and/or lithologies. Low gamma-ray cps usually correspond to organic-poor lithologies, such as quartz sandstones.

In the studied section, gamma-ray cps varies from 92.6 to 246.4 cps (Figure 3.4). The low cps mostly corresponds to the sandstone beds, while the higher cps values were recorded in the shales and coals. The high gamma-ray values in the red shale beds is most likely due the presence of potassium-feldspars or heavy minerals containing U, Th and K, since they are not visibly rich in organic matter. One of the sandstones also presented high natural radioactivity, also likely due to the presence of potassium-feldspars or heavy minerals containing U, Th and K. The contrast between low and high gamma-ray values in a single sandstone bed suggest the existence of heterogeneous lithofacies within a single sandbody.

4.3 Integrated Reservoir Characterization

By using the DOM, the architecture of the channels can be measured. The thickness of these channels were measured to be approximately 8 m, 23 m and 8 m thick (Figure 4.4). Within the 23 m reservoir section a number of baffle and barriers exists as interbedded shales (gray colour) (Figure 4.4). The ends of this channel bodies could not be measured as these units disappeared beneath the intertidal zone and were truncated by the unconformity on the top. Within the interbedded zone (Figure 4.4), we can identify false connectivity which appears to the increase to the net to gross sand to shale. Gamma-ray identifies the different lithologies observed at outcrop and identifies low cps reservoirs (sands) and high cps seals and baffles (shales/coals). Gamma-ray values (cps), combined with digital photography, corrects the interpretation of recorded intensity data from lidar. Assessment of reservoir connectivity at the outcrop scale, using the DOM, indicates poor reservoir connectivity. Connected channel bodies are very important for a hydrocarbon reservoirs or aquifers, as this increases the size of the reservoir body and aids in production.

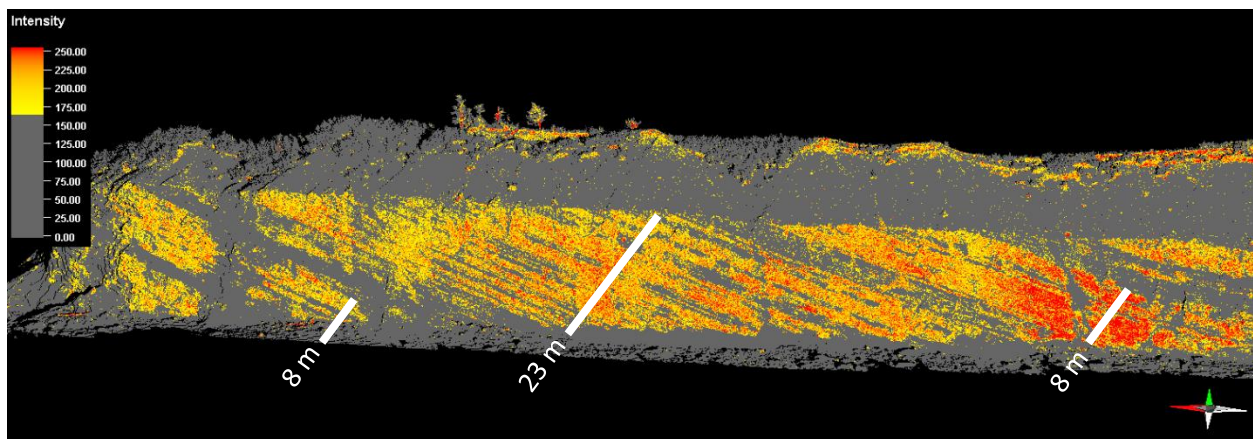


Figure 4.4 - Petrel render image of the data set, measuring 3 different reservoirs separated by thick shales. The reservoirs units are noted to be 8 m, 23 m and 8 m. Within each reservoir shale baffles and barriers are noted to separate connectivity between sandstone channels.

5 Conclusion and Recommendation

5.1 Conclusion

The objectives of this work were to answer the following questions:

- a) Is lidar capable of aiding in the identification of different lithological successions?

As previously known lidar survey is a technique which is capable of capturing 3D point cloud images of outcrop. This data can be used for identifying different lithological units within the outcrop. This can be a very powerful tool for differentiating different types of units using a digital outcrop model. In addition, using the digital outcrop model it is possible to visualize the connectivity of the sand bodies as it is very important to understand them for potential reservoirs; integration with additional data such as permeability or gamma-ray, enhanced analysis of the outcrop, identifying seal or reservoir rocks and its spatial geometry and. At the studied location, it is deduced that the sand bodies present low permeability with baffle and flows.

- b) Can lidar identify fossilized trees within the Joggins Formation?

Lidar survey has the capability to capture 3D point cloud data of outcrops at a very high resolution. Fossil tree geometries are identifiable in the digital outcrop model, although always aided by field work and digital photography. At this stage, lidar is not a suitable to be used as a standalone tool to identified fossilized trees.

- c) Can lidar help characterize reservoir connectivity in meander belt systems?

Lidar survey can help characterize the reservoir connectivity in meander belt systems, as observed in the illustration (Figure 3.5) the channel bodies can be defined by the high values of intensity, although error corrections have to be considered during the data collection and processing of the digital outcrop model as discussed previously about irregular outcrop geometries.

- d) Can lidar data integrated with outcrop observation, gamma-ray and permeability data aid in the interpretation of stratigraphical and sedimentological features of hydrocarbon reservoirs?

Lidar provided important information for rock properties (intensity) and high detail of the outcrop that can used in the assessment of the reservoir characteristics of the Joggins Formation in Coal Mine Point section. In this study we observed that higher intensity values corresponds to sandbodies and low intensity values corresponds to shales in the digital outcrop model. The digital outcrop model provided data about reservoir connectivity and

lithofacies. Demonstrating the sand bodies have high permeability (Table 3.6) and usually low gamma values and connectivity.

5.2 Recommendations and Future Work

It is recommend completing lidar scans of the Coal Mine Point reference section annually or semi-annually to generate a point cloud data set for Vertical Time Slices, and process the data collected. This iterative process will create a 3D model with the Vertical Times Slices (Figure 5.1). More scans of the area, from different points of view, will lower the amount of shadow zones, enhancing the data set with more features that are captured with only a single point of view. It is also recommended to have a hygrometer measure the humidity and thermometer to measure the temperature when the lidar scan is being scanned. It is important to ensure that the weather conditions are favorable for the survey to be performed, as tides and weather can limit the timeframe of survey scanning. As discussed in section 4.1.1.

3D model over time will provide greater understanding of this part of the Cumberland Basin, and the reconstruction of the forest dynamics during the Carboniferous. As previously mention sedimentation rates where high during the Carboniferous. This is very noticeable and distinctive at outcrop, but with a 3D model of the meander channels we can calculate and understand the complex interplay of halokinesis and sedimentation rates in the Cumberland Basin. Additionally, aiming at coastal risk assessment and mitigation, the obtained data will contribute to the understanding and quantification of coastal erosion at the Joggins Fossil Cliffs. This evaluation will pinpoint risk areas for future development of the region. The digital outcrop model can also be used for different purposes, for example, in CO₂ sequestration studies that are currently being planned for carboniferous channel bodies in the Sydney Basin (CCS Nova Scotia, 2014).

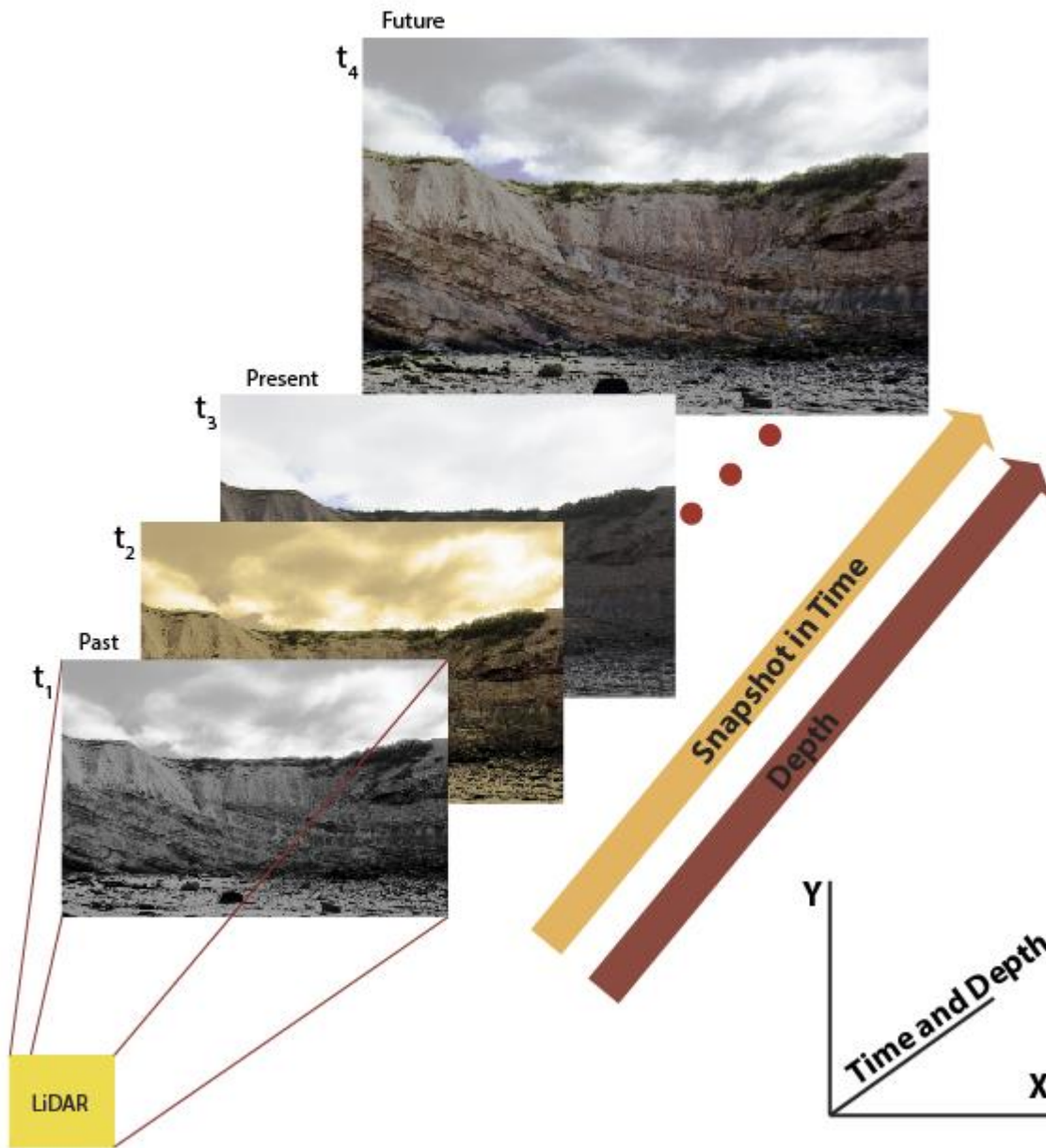


Figure 5.1 – To build a 3D model of the study area multiple scans must be completed and compiled to both generate a true representation of the Joggins Formation and to measure coastal erosion rates.

Multiple scans must be completed through time and compiled to generate a 3D model.

5.2.1 3D Visualization

Other 3D visualization software can be more useful for the developing of the 3D digital outcrop model, currently Petrel has its limitation. More dedicated software to build 3D models are in the market such as Polyworks, GOCAD, and these should be tested.

With this 3D digital outcrop model, the Joggins Fossil Cliff Centre can use as a base model to recreate a 3D virtual environment during the Carboniferous and use it at the Joggins Fossil Cliff Centre as a virtual tour for their visitors with very accurate representation of the carboniferous past and present at Joggins. 3D environments can be developed as a virtual tour for future visitors at the Joggins Fossil Cliff Centre, increasing interactivity. Many other applications can be built with the vertical time slice, such as augmented reality applications to highlight what tourists can see during tours. Augmented Reality (AR) is a view of the real world environment with elements that are augmented by computer generated sensors, such as sound, video, graphics and GPS data. Eyeglasses like Google glass can be used and programed to provide an AR tour of the Joggins outcrop, with a guide pointing out the areas of interest making the tour more interactive and informative for them. Such wearable technology is still in development, but will be available in near future. Augmented Reality using eye glasses displays images in real time, with a LCD projection, of the cliff. This technology of AR is been applied for multiple uses such as a digital manual for a car manufacturer (Figure 5.2). Although accessible for able-bodied individuals, elderly and handicapped visitors have limited access to the cliff section. An interactive 3D tour of the cliff will allow visitors to enjoy the wonders of the Carboniferous landscapes preserved at Joggins.



Figure 5.2 – A car service manual using augmented reality (Aol Tech., 2014).

6 References

- Aol Tech. (2014, 3 14). *Volkswagen develops augmented reality service manual for the XL1*. Retrieved from Engadget: <http://www.engadget.com/2013/10/01/volkswagen-augmented-reality-ipad-manual-xl1/>
- Apple Inc. (2014, 3 14). Maps.
- Bellian, J., Kerans, C., & Jennette, D. (2005). Digital Outcrop Models: Applications of Terrestrial Scanning Lidar Technology in Stratigraphic Modeling. *Journal of Sedimentary Research*, 75(2), 166-176.
- Buckley, S., Kurz, T., Howell, J., & Schneider, D. (2013). Terrestrial lidar and hyperspectral data fusion products for geological outcrop analysis. *Computers & Geosciences*, 54, 249-258.
- Burton, D., & Wood, L. (2010). Lidar Intensity as a Remote Sensor of Rock Properties. *Annual Rocky Mountain Rendezvous*. Austin: AAPG Rocky Mountain Section 58th.
- Burton, D., Dunlap, D., Wood, L., & Flaig, P. (2011). Lidar Intensity as a Remote Sensor of Rock Properties. *Journal of Sedimentary Research*, 81, 339-347.
- Calder, J. (2012). *The Joggins Fossil Cliffs: Coal Age Galapagoes*. Halifax: Communications Nova Scotia for the Nova Scotia Department of Natural Resources.
- Calder, J. H. (2006). A fossil lycopsid forest successio in the classic Joggins section of Nova Scotia: Paleoeecology of a disturbance-prone Pennsylvanian wetland. In S. F. Greb, & W. A. DiMichele, *Wetlands through Time* (pp. 169-195). Boulder: The Geological Society of America.
- Campos, L., Veronez, M., Wohnrath, F., Souza, M., Silva, R., Gonzaga, L., & Blum, C. (2013). Spectral Pattern Classification in Lidar Data for Rock Identification in Outcrops. *The Scientific World Journal*, 2014, 10.
- CCS Nova Scotia. (2014). *Carbon Capture and Storage Nova Scotia*. Retrieved 03 14, 2014, from <http://www.ccsnovascotia.ca/>
- Davies, S., & Gibling, M. (2003). Architecture of coastal and alluvial deposits in an extensional basin: the Carboniferous Joggins Formation of eastern Canada. *Sedimentology*, 50, 415-439.

- Davies, S., Gibling, M., Rygel, M., Calder, J., & Skilliter, D. (2005). The Pennsylvanian Joggins Formation of Nova Scotia: sedimentological log and stratigraphic framework of the historic fossil cliffs. *Atlantic Geology*, *41*, 115-142.
- Fensome, R. A., & Williams, G. L. (2001). *The Last Billion Years - A Geological History of the Maritime Provinces of Canada*. (R. A. Fensome, & G. L. Williams, Eds.) Halifax, Canada: Nimbus Publishing.
- Google Inc. (2014, 3 14). Google Earth.
- Grey, M., & Finkel, Z. (2011). The Joggins Fossil Cliffs UNESCO World Heritage site: a review of recent research. *Atlantic Geology*, *47*, 185-200.
- Hartzell, P., C., G., Biber, K., & Khan, S. (2014). Application of multispectral LiDAR to automated virtual outcrop geology. *ISPRS Journal of Photogrammetry and Remote Sensing*, 147-155.
- Hobbs, P., Gibson, A., Pennington, C., Jenkins, G., Pearson, S., & Freeborough, K. (2010). Monitoring coastal change using terrestrial LiDAR. *The Geological Society of London*, *345*, 117-127.
- Jackson, M., Vendeville, B., & Schultz-Ela, D. (1994). Structural Dynamics of Salt Systems. *Annual Review Of Earth And Planetary Sciences*, *22*, 93-117.
- Kelly, T. (2013). *Lidar Image*. Joggins, Nova Scotia, Canada.
- McCabe, P. (1991). Tectonic control on coal accumulation. *Bulletin de la Societe Geologique de France*, *162*(2), 277-282.
- Miall, A. (2010). Alluvial Deposits. In N. P. James, & R. W. Dalrymple (Eds.), *Facies Models 4* (pp. 105-137). St. John's: Geological Association of Canada.
- National Coordination Office for Space-Based Positioning, Navigation, and Timing. (2014, 02 21). *GPS Accuracy*. Retrieved from Official U.S. Government information about the Global Positioning System (GPS) and related topics: <http://www.gps.gov/systems/gps/performance/accuracy/>
- Nebaway, B., Rochette, P., & Geraud, Y. (2009). Petrophysical and magnetic pore network anisotropy of some cretaceous sandstone from Tushka Basin, Egypt. *Geophysics Journal International*(177), 43-61.
- New England Research Inc. (n.d.). *TinyPerm II Potable Air Permeameter User's Manual*.
- O'Connor, D. (2013). *LiDAR Image*.

- Prothero, D. R., & Schwab, F. (2004). *Sedimentary Geology: An Introduction to Sedimentary Rocks and Stratigraphy*. New York: W.H. Freeman and Company.
- Rafuse, C., & Wach, G. (2011). *Reservoir architecture of meanderbelt systems and vegetation density in Carboniferous using LIDAR imagery*. Undergraduate directed studies project, Dalhousie University, Department of Earth Sciences, Canada.
- Reading, H. G. (1996). *Sedimentary Environments: Processes, Facies and Stratigraphy* (3rd ed.). Wiley-Blackwell.
- Rygel, M. (2010). *Alluvial Architecture of the Springhill Mines and Ragged Reef Formations: Fluvial Reservoir Characteristics Linked to Paleogeomorphology*. State University of New York at Potsdam. American Chemical Society.
- Rygel, M. C. (2005). *Alluvial sedimentology and basin analysis of Carboniferous strat near Joggins, Nova Scotia, Atlantic Canada*. Halifax: Dalhousie University.
- Schlumberger. (2014). *Gamma Ray Log*. Retrieved from Oilfield Glossary: <http://www.glossary.oilfield.slb.com/en/Terms.aspx?LookIn=term%20name&filter=gamma%20ray%20log>
- Slatt, R., Jordan, D., & D'Agostino, A. (1992). Outcrop gamma-ray logging to improve understanding of subsurface well log correlations. *The Geological Society of London*, 65, 3-19.
- Thomas, B. A. (2012). In situ stems: preservation states and growth habits of the Pennsylvanian (Carboniferous) calamitaleans based upon new studies of Calamites Sternberg, 1820 in the Duckmantian at Brymbo, North Wales, UK. *The Palaeontological Association*, 57, 21-36.
- Waldron, J., & Rygel, M. (2005, May). Role of evaporite withdrawal in the preservation of a unique coal-bearing succession: Pennsylvanian Joggins Formation, Nova Scotia. *Geology*, 33(5), 337.

7 Appendix

7.1 Complete measured stratigraphic section of the Joggins Formation at Coal Mine Point

(stratigraphical section from Rygel, 2005).

